Cell Reports

Supplemental Information

Accumulation of Basic Amino Acids at Mitochondria Dictates the Cytotoxicity of Aberrant Ubiquitin

Ralf J. Braun, Cornelia Sommer, Christine Leibiger, Romina J.G. Gentier, Verónica I. Dumit, Katrin Paduch, Tobias Eisenberg, Lukas Habernig, Gert Trausinger, Christoph Magnes, Thomas Pieber, Frank Sinner, Jörn Dengjel, Fred W. van Leeuwen, Guido Kroemer, and Frank Madeo

Supplemental Information

Supplemental Items Inventory

- *Supplemental Figures and Legends*
  - Figure S1 (related to Figure 1)
    Expression of UBB^{+1} in yeast and its effect on proteasomal activities
  - Figure S2 (related to Figure 2)
    Stressors elevating UBB^{+1}-triggered cytotoxicity, and markers of oxidative stress, apoptosis and necrosis
  - Figure S3 (related to Figure 3)
    UBB^{+1}-triggered cytotoxicity in yeast strains with various UPS capacities, and expression controls
  - Figure S4 (related to Figure 4)
    Mitochondrial impairment upon UBB^{+1} expression, respiratory and expression capacities of strains deleted for cell death genes
  - Figure S5 (related to Figure 5)
    Cytotoxicity of UBB^{+1} in strains with disrupted arginine/ornithine biosynthesis
  - Figure S6 (related to Figure 6)
    Role of Cdc48/Npl4/Vms1 complex in UBB^{+1}-triggered cytotoxicity and steady-state levels of UBB^{+1}
  - Figure S7 (related Figure 7)
    Pathological hallmarks in AD patients, and in non-demented controls
- *Supplemental Tables*
  - Table S1 (related to Figures 1-6)
    Data pooling and statistics
  - Table S2 (related to Figure 5)
    Protein alterations in crude mitochondrial extracts upon expression of UBB^{+1}
  - Table S3 (related to Figure 6)
    Protein alterations in crude mitochondrial extracts upon expression of UBB^{+1} and increased levels of Vms1
  - Table S4 (related to Tables S2+S3)
    Protein identifications and quantification by SILAC analysis of crude mitochondrial extracts
  - Table S5 (related to Figure 7)
    Immunoreactivities in the human hippocampus and entorhinal cortex for VMS1
  - Table S6 (related to Figures 7+S7 and Table S5)
    Clinico-pathological information of non-demented controls and AD patients
- *Supplemental Discussion*
- *Supplemental Experimental Procedures*
- *Supplemental References*
- *Detailed Author Contributions*

Supplemental Figures and Legends

Figure S1 (related to Figure 1):

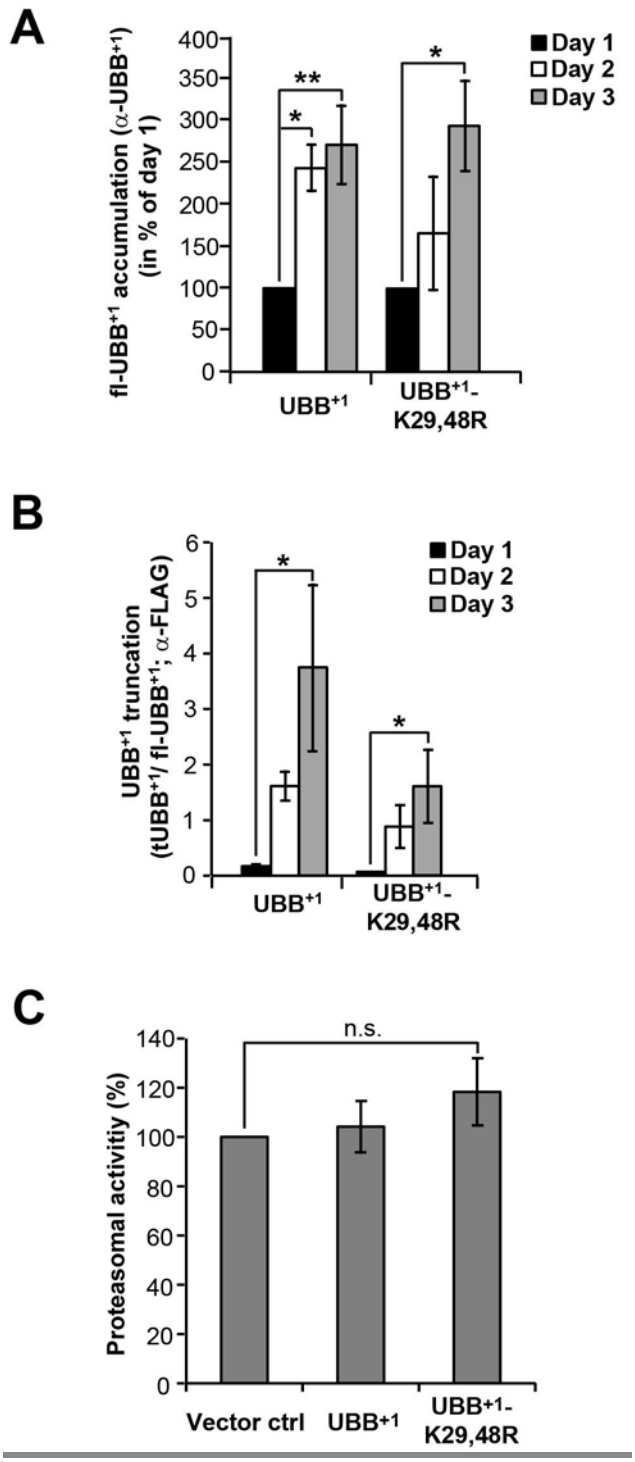

Figure S1: Expression of UBB^{+1} in yeast and its effect on proteasomal activities

(A+B) Expression of UBB^{+1} as in Figure 1A. (A) Accumulation of UBB^{+1} was determined by the quantification of immunoblots of cell extracts using antibodies directed against the specific C-terminus of UBB^{+1} and hexokinase (Hxk) as loading control. Full-length UBB^{+1} (fl-UBB^{+1}) levels at day 1 were set to 100% in every experiment. The data shown here are percent change values of five independent experiments. Error bars: standard error. *p < 0.05, **p < 0.01 (ANOVA/ Bonferroni t-test).

(B) Truncation of UBB^{+1} was determined by the quantification of immunoblots of cell extracts using an antibody directed against the N-terminal FLAG-tag of UBB^{+1}. The data shown here are mean values of five independent experiments. fl-UBB^{+1}: full-length UBB^{+1}, tUBB^{+1}: truncated UBB^{+1}. Error bars: standard error. *p < 0.05 (ANOVA on ranks/ Dunn's method).

(C) UBB^{+1} was expressed overnight. Cultures were diluted in expression medium, grown to logarithmic phase, and chymotrypsin-like proteasomal activities were determined. The proteasomal activities obtained using yeast cells expressing vector controls were set to 100% in every experiment. The data shown here are percent change values of four independent experiments. Error bars: standard error. n.s.: not significant (ANOVA).

Figure S2 (related to Figure 2):

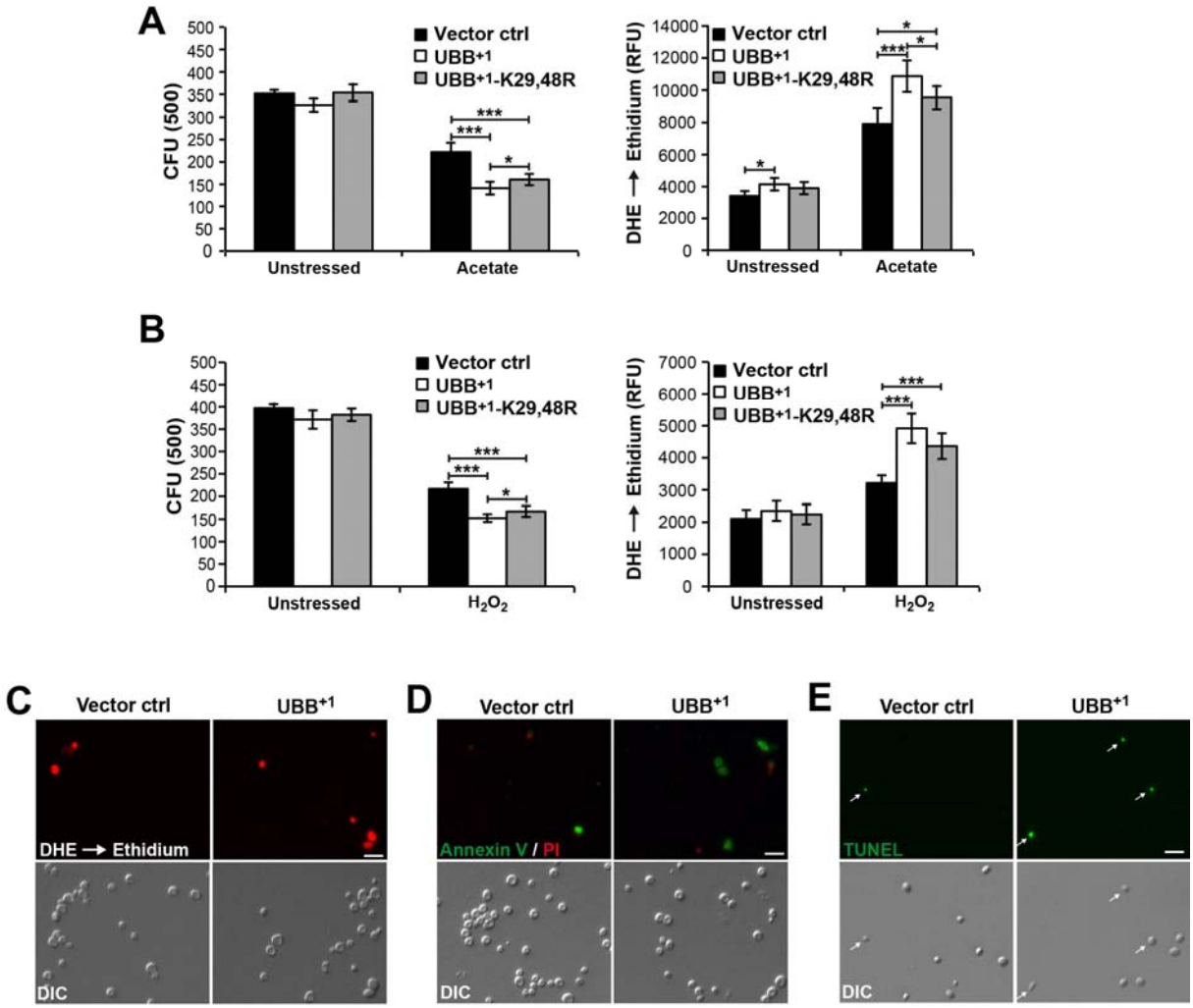

Figure S2: Stressors elevating UBB^{+1}-triggered cytotoxicity, and markers of oxidative stress, apoptosis and necrosis

(A+B) Sensitivity against mitochondrial stressors upon UBB^{+1} expression. Two days after inducing expression, yeast cultures were treated for 4 h either with 140 mM acetate (A), or 2.8 mM hydrogen peroxide (H_2O_2) (B). *Left panels:* Measurement of clonogenicity. *Right panels:* Measurement of oxidative stress (DHE staining) using a fluorescence plate reader. The data shown here are mean values of six and nine independent experiments for (A) and (B), respectively. Error bars: standard error. p-values: *p < 0.05, **p < 0.01, ***p < 0.001 (RM ANOVA/ Holm-Sidak method).

(C-E) Fluorescence microscopic analysis of DHE- (C), Annexin V/PI- (D), and TUNEL- (E) stained cells described in Figure 2D-F. Scale bar: 10 µm.

Figure S3 (related to Figure 3):

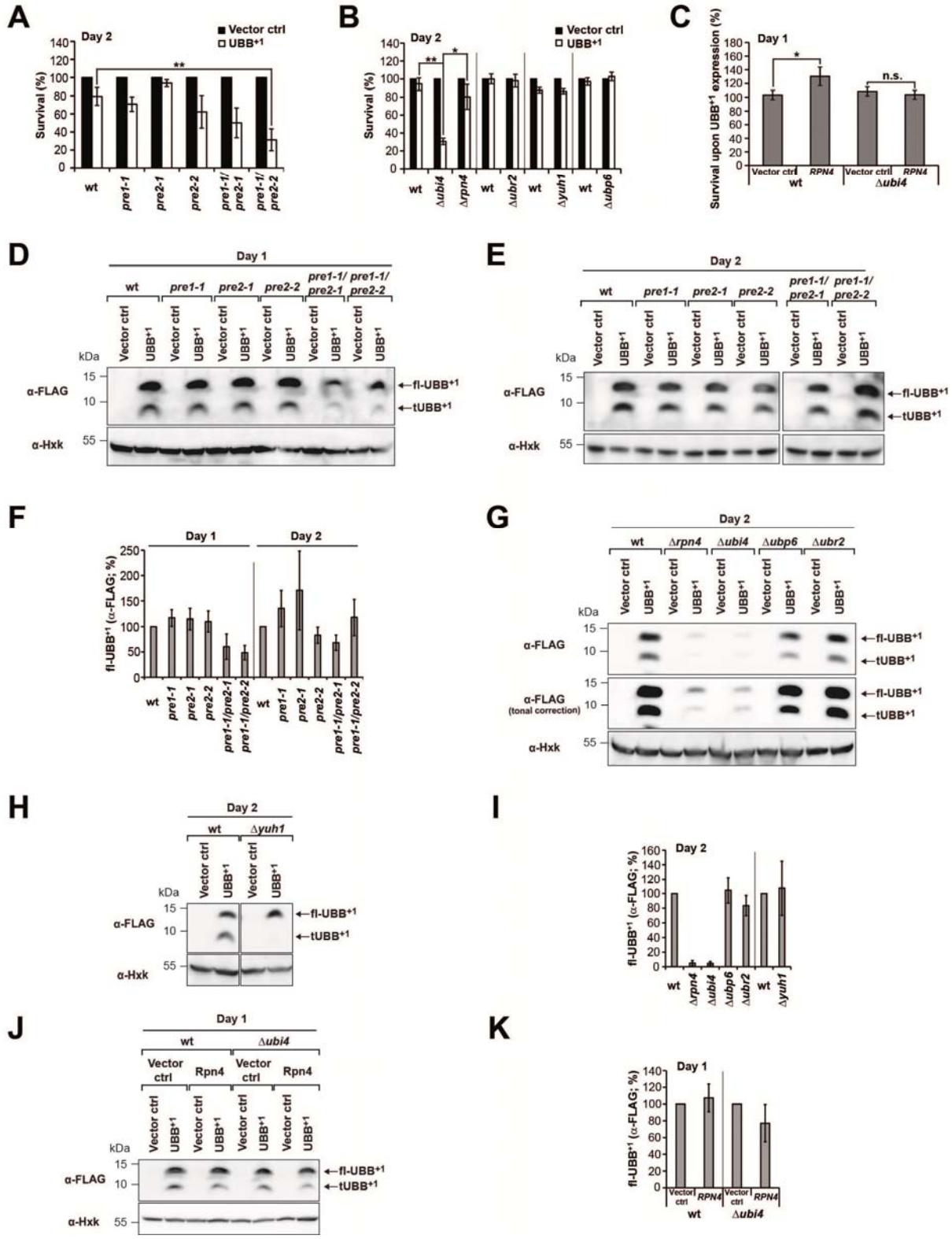

Figure S3: UBB^{+1}-triggered cytotoxicity in yeast strains with various UPS capacities, and expression controls

(A) Clonogenicity in proteasomal mutant strains. The CFUs obtained using yeast cells expressing vector controls were set to 100% in every experiment. The data shown here are

percent change values of four independent experiments for day 2 (for day 1 see Figure 3B). Error bars: standard error. **p < 0.05 (paired t-test).

(B) Clonogenicity in selected UPS knock-out strains. Unstressed controls to Figure 3D. Error bars: standard error. *p < 0.05, **p < 0.01 (paired t-test).

(C) UBB^{+1} was expressed in wild-type and Δ*ubi4* strains with endogenous (vector control) and elevated levels of Rpn4 (Rpn4). Clonogenicity was determined 1 day after inducing expression. The CFUs obtained using yeast cells with endogenous and elevated levels of Rpn4, respectively, but lacking UBB^{+1}, were set to 100% in every strain and experiment (not shown). The data shown here are percent change values of eight and six independent experiments for wt and Δ*ubi4* strains, respectively. Error bars: standard error. *p ≤ 0.05 (paired t-test).

(D-F) Steady-state levels of UBB^{+1} in proteasomal mutant strains upon expression for 1 (D) and 2 (E) days, respectively (relevant for Figures 3B and S3A). (F) Quantification of UBB^{+1} levels was done by immunoblotting of cell extracts using an antibody directed against the N-terminal FLAG-tag of UBB^{+1}. Hexokinase (Hxk) was used as loading control. The immunoreactive signals obtained using wild-type cells were set to 100% in every experiment. The data shown here are percent change values of three independent experiments. fl-UBB^{+1}: full-length UBB^{+1}. Error bar: standard error.

(G-I) Steady-state levels of UBB^{+1} in selected UPS knock-out strains upon expression for 2 days (relevant for Figures 3D and S3B). (I) Quantification of UBB^{+1} levels was done as in (F). The data shown here are percent change values of three independent experiments. fl-UBB^{+1}: full-length UBB^{+1}. Error bar: standard error.

(J+K) Steady-state levels of UBB^{+1} upon endogenous and elevated levels of Rpn4 in wild-type and Δ*ubi4* strains (relevant for Figures 3F and S3C). UBB^{+1} and Rpn4 were expressed for 1 day. Hexokinase (Hxk) was used as loading control. The immunoreactive signals obtained using wild-type yeast cells were set to 100% in every experiment. The data shown here are percent change values of three independent experiments. fl-UBB^{+1}: full-length UBB^{+1}. Error bar: standard error.

Figure S4 (related to Figure 4):

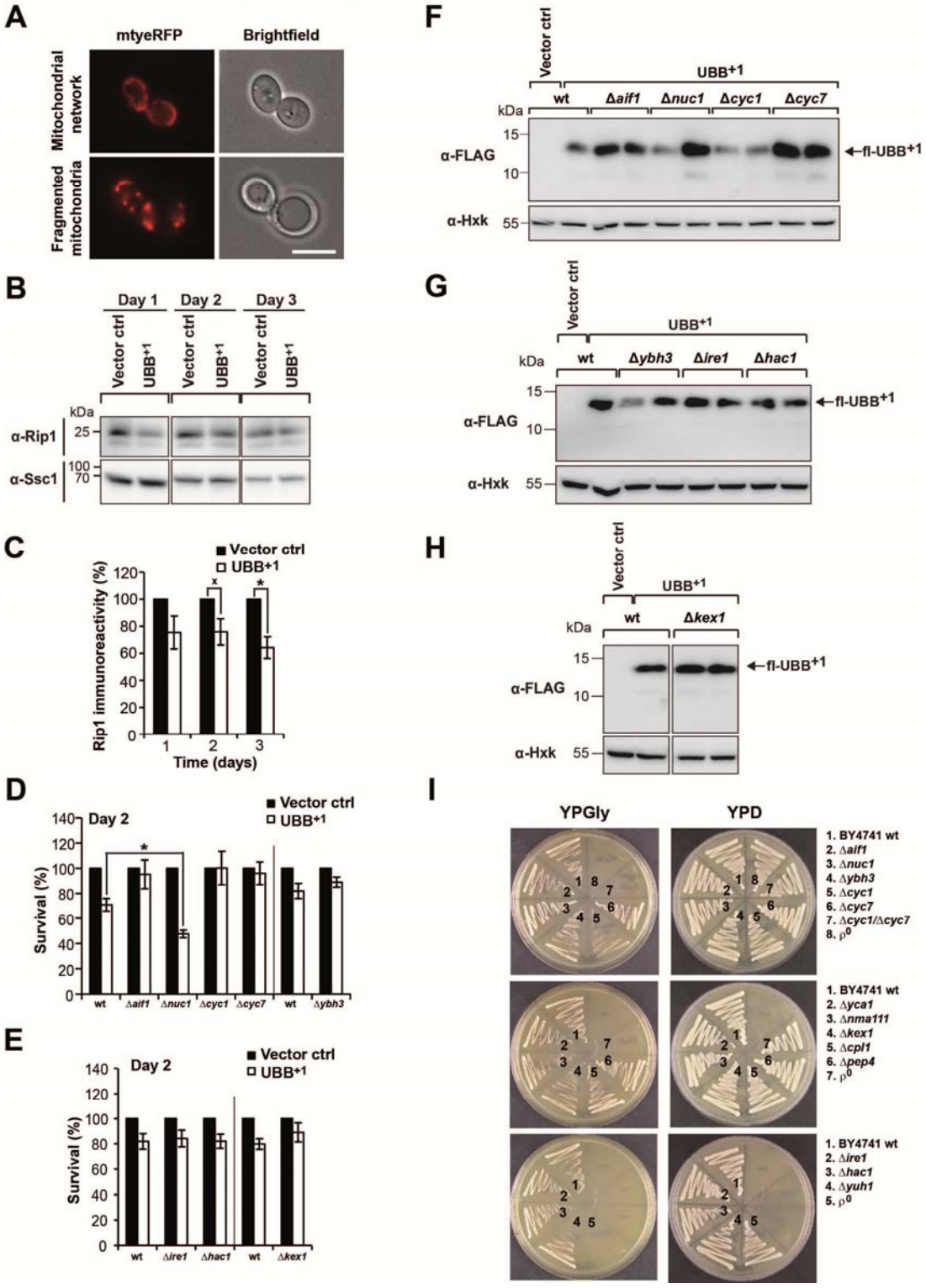

Figure S4: Mitochondrial impairment upon UBB^{+1} expression, respiratory and expression capacities of strains deleted for cell death genes

(A) Mitochondrial fragmentation. UBB^{+1} and a red fluorescent protein (yeRFP) fused with a mitochondrial targeting sequence were expressed. Representative images showing cells with

intact mitochondrial network, and with fragmented mitochondria, respectively. Size bar: 5 µm.

(B+C) Protein alterations in cell extracts. Proteins were expressed for 1 (16 h), 2, or 3 days. Steady-state levels of the mitochondrial cytochrome bc_1 complex component Rip1 and the mitochondrial chaperone Ssc1 were determined by immunoblotting of cell extracts. (B) Representative immunoblot. (C) Quantification of Rip1. Rip1 amount was normalized to Ssc1, and Rip1/Ssc1 was set to 100% in every experiment. The data shown here are percent change values of four experiments done in parallel. Error bars: standard error. p-values: $^{x}p < 0.1$, $*p < 0.05$ (paired t-test).

(D) Cytotoxicity in strains deleted from genes encoding mitochondrial cell death proteins. Unstressed controls to Figure 4H. Error bars: standard error. $*p \leq 0.05$ (paired t-test).

(E) Cytotoxicity in strains deleted from genes encoding ER-associated proteins. Unstressed controls to Figure 4I. Error bars: standard error.

(F-H) UBB^{+1} expression control in yeast strains (relevant for Figures 4H, 4I, S4D, S4E). UBB^{+1} was expressed in the indicated yeast strains for 16 h (day 1). Steady-state levels of UBB^{+1} were determined by immunoblotting. Hexokinase (Hxk) was used as loading control. Please note: Two distinct expression clones were shown per knock-out strain. fl-UBB^{+1}: full-length UBB^{+1}.

(I) Respiratory growth of yeast strains (relevant for Figures 4H, 4I, S4D, S4E). The indicated yeast strains were streaked out on YP plates with glycerol (YPGly) and glucose (YPD) as sole carbon sources, respectively, enabling obligatory respiratory and fermentative growth. ρ^0 strains and Δ*cyc1*/Δ*cyc7* double knock-out strain were used as controls for respiratory deficiency.

Figure S5 (related to Figure 5):

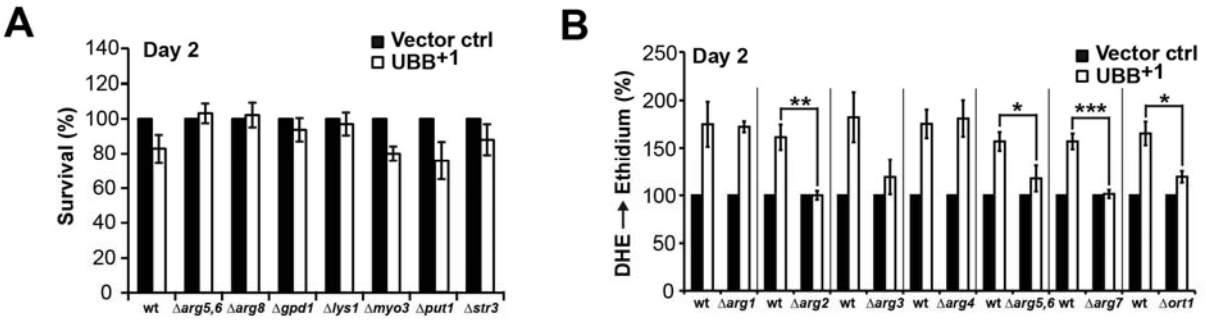

Figure S5: Cytotoxicity of UBB^{+1} in strains with disrupted arginine/ornithine biosynthesis

(A) UBB^{+1}-triggered cytotoxicity in strains deleted from genes encoding proteins accumulating in crude mitochondrial extracts upon UBB^{+1} expression. Unstressed controls to Figure 5B. Error bars: standard error.

(B) Oxidative stress upon UBB^{+1} expression in yeast strains with disrupted arginine/ornithine biosynthesis. Unstressed controls to Figure 5E. Error bars: standard error. *$p < 0.05$, **$p < 0.01$, ***$p < 0.001$ (t-test).

Figure S6 (related to Figure 6):

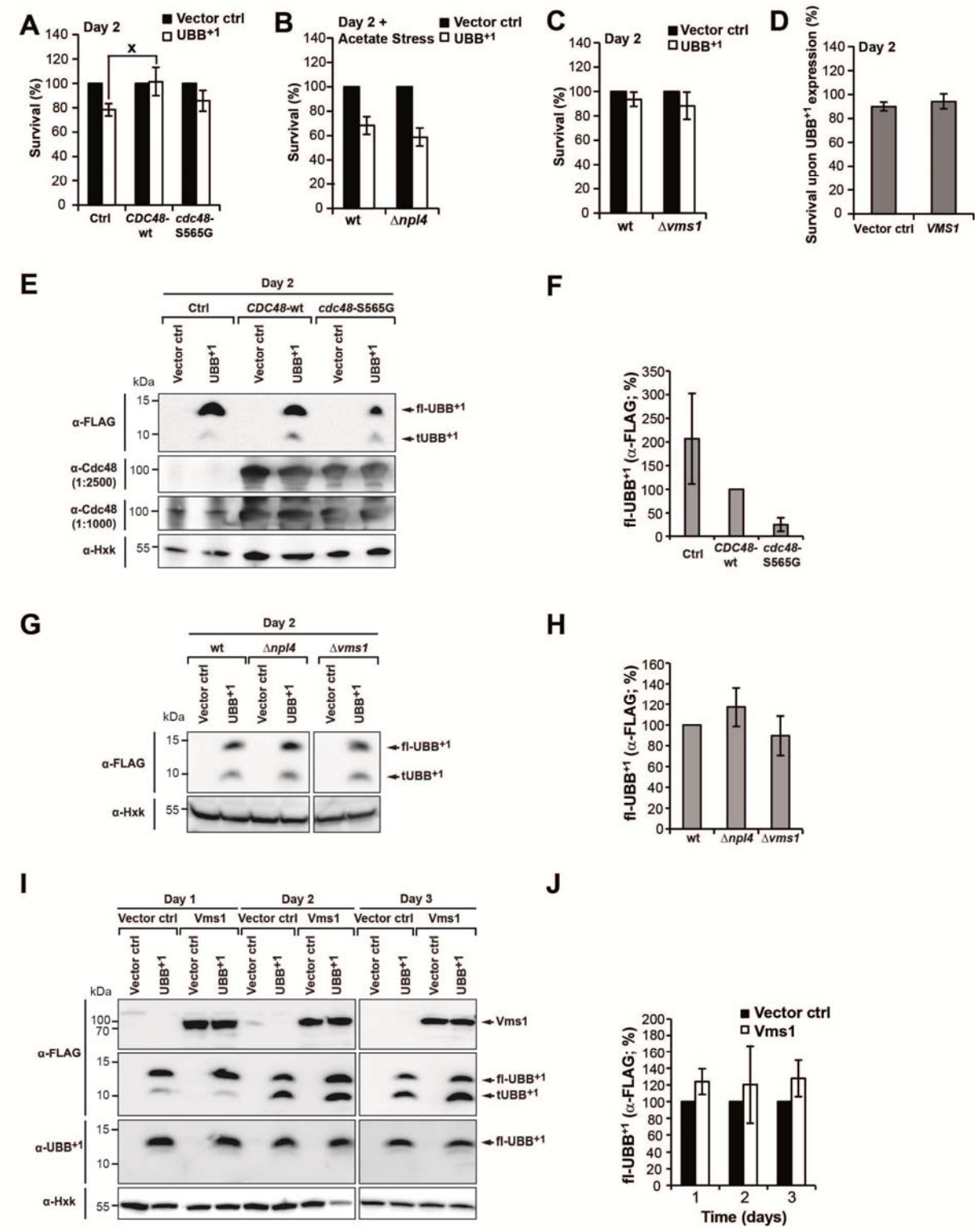

Figure S6: Role of Cdc48/Npl4/Vms1 complex in UBB^{+1}-triggered cytotoxicity and steady-state levels of UBB^{+1}

(A-C) UBB^{+1} was expressed in yeast strains with elevated levels of Cdc48 or Cdc48-S565G (A), and strains deleted for *NPL4* (B) and *VMS1* (C). Clonogenicity was determined two days after inducing expression before (A, C) and after acetate stress (B) (controls to Figure 6A-C).

The CFUs obtained using yeast cells expressing vector controls were set to 100% in every experiment. The data shown here are percent change values of six (A, B), and four (C) independent experiments. Error bars: standard error. $^{x}p < 0.1$ (paired t-test).

(D) Clonogenicity of UBB^{+1}-expressing cultures in strains with endogenous (vector control) and elevated levels of Vms1 (Vms1), respectively. Unstressed controls to Figure 6D. Error bars: standard error.

(E+F) Steady-state levels of UBB^{+1} and Cdc48 (relevant for Figures 6A, S6A). Hexokinase (Hxk) was used as loading control. (F) fl-UBB^{+1} levels in the *CDC48*-wt strain were set to 100% in every experiment. The data shown here are percent change values of three independent experiments. Error bars: standard error.

(G+H) Steady-state level of UBB^{+1} (relevant for Figures 6B+C, S6B+C). Hexokinase (Hxk) was used as loading control. (H) fl-UBB^{+1} levels in wt strain were set to 100% in every experiment. The data shown here are percent change values of three independent experiments. Error bars: standard error.

(I+J) Steady-state level of UBB^{+1} and Vms1 (relevant for Figures 6D-F, S6D). UBB^{+1} and/or Vms1 were expressed for 1 day (16 h), 2 and 3 days. Steady-state levels of Vms1 were determined by immunoblotting of cell extracts using an antibody directed against the C-terminal FLAG-tag of Vms1. Steady-state levels of UBB^{+1} were determined using an antibody directed against the N-terminal FLAG-tag of UBB^{+1} or directed against the UBB^{+1}-specific C-terminus. Hexokinase (Hxk) was used as loading control. (J) fl-UBB^{+1} levels in strains with endogenous levels of Vms1 (vector ctrl) were set to 100% in every experiment. The data shown here are percent change values of six experiments. Error bars: standard error. fl-UBB^{+1}: full-length UBB^{+1}, tUBB^{+1}: truncated UBB^{+1}.

Figure S7 (related Figure 7)

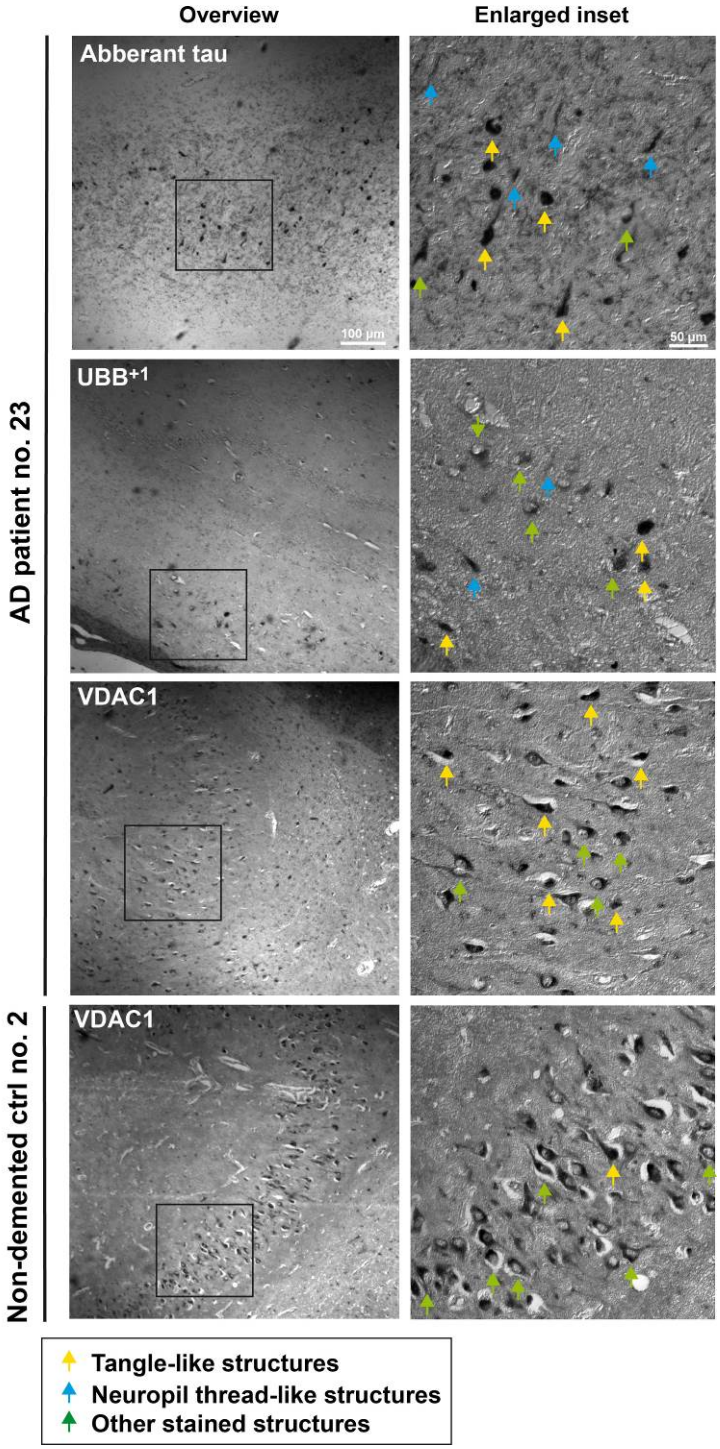

Figure S7: Pathological hallmarks in AD patients and in non-demented controls

Aberrant tau, UBB^{+1}, and VDAC1 staining in hippocampi of an AD patient.

Table S1 (related to Figures 1-6):

Data pooling and statistics

(see also Statistics in Supplemental Experimental Procedures)

Figure	Data	Error bars	Statistics
Figure 1C	Percent change values of five independent experiments	Standard error	ANOVA on ranks/ Dunn's method
Figure 1D	Mean values of nine, eight, and four independent experiments for days 1, 2, and 3, respectively	Standard error	RM ANOVA on ranks/ Dunn's method
Figure 2B	Mean values of three experiments done in parallel	Standard deviation	-
Figure 2C	Mean values of 20, 28, and 10 independent experiments for days 1, 2, and 3, respectively	Standard error	RM ANOVA/ Holm-Sidak method
Figure 2D	Mean values of 15, 25, and 5 independent experiments for days 1, 2, and 3, respectively	Standard error	RM ANOVA/ Holm-Sidak method
Figure 2E+F	Mean values of eight independent experiments	Standard error	RM ANOVA/ Holm-Sidak method
Figure 3A	Percent change values of three independent experiments	Standard error	RM ANOVA/ Holm-Sidak method
Figure 3B	Percent change values of three independent experiments	Standard error	Two-tailed paired t-test
Figure 3C	Percent change values of three, three, and four independent experiments for wt/Δ*ubi4*/Δ*rpn4*, wt/Δ*yuh1*, and wt/Δ*ubp6*, respectively	Standard error	RM ANOVA/ Holm-Sidak method
Figure 3D	Percent change values of four, four, five, and eight independent experiments for wt/Δ*ubi4*/Δ*rpn4*, wt/Δ*yuh1*, and wt/Δ*ubp6*, respectively	Standard error	Two-tailed paired t-test
Figure 3E	Percent change values of three independent experiments	Standard error	Two-tailed unpaired t-test
Figure 3F	Percent change values of four independent experiments	Standard error	Two-tailed paired t-test
Figure 4A	Mean values of nine independent experiments	Standard error	Two-tailed paired t-test
Figure 4B	Mean values of twelve independent experiments. At least 500 cells were evaluated per experiment and condition	Standard error	Two-tailed paired t-test
Figure 4C	Percent change values of four and three independent experiments for days 2 and 3, respectively	Standard error	Two-tailed unpaired t-test
Figure 4D	Percent change values of five and four independent experiments for days 2 and 3 respectively	Standard error	Rank Sum Test
Figure 4E	Percent change values of four independent experiments	Standard error	Rank Sum Test
Figure 4G	Percent change values of five independent experiments	Standard error	Two-tailed unpaired t-test
Figure 4H	Percent change values of five and seven independent experiments for wt/Δ*aif1*/Δ*nuc1*/Δ*cyc1*/Δ*cyc7* and wt/Δ*ybh3*, respectively	Standard error	Two-tailed paired t-test
Figure 4I	Percent change values of seven and four independent experiments for wt/Δ*ire1*/Δ*hac1* and wt/Δ*kex1*, respectively	Standard error	Two-tailed paired t-test
Figure 5B	Percent change values of four, and five independent experiments for Δ*gpd1*, Δ*put1*, Δ*str3*, Δ*myo3* and wild-type, Δ*arg5,6*, Δ*arg8*, Δ*lys1*, respectively	Standard error	ANOVA/ Holm-Sidak method
Figure 5C	Mean values of four experiments done in parallel (in each case two performed with the acid and two with the hot ethanol extraction methods)	Standard error	Two-tailed unpaired t-test
Figure 5E	Percent change values of three independent experiments for wt/Δ*arg1* and wt/Δ*arg3* and five independent experiments for the other comparisons	Standard error	Two-tailed unpaired t-test
Figure 5F	Percent change values of three, eight, two, one, five and five independent experiments for growth media without arginine (w/o) and with 30, 50, 75, 150, and 300 mg/L arginine, respectively	Standard error	Two-tailed unpaired t-test
Figure 5G	Percent change values of three and six independent experiments for growth media without lysine (w/o) and with 30, 80, 150, and 300 mg/L lysine	Standard error	Two-tailed unpaired t-test
Figure 6A-C	Percent change values of sic (A), eight (B), and four (C) independent experiments	Standard error	Two-tailed paired t-test
Figure 6D	Percent change values of six independent experiments	Standard error	Two-tailed paired t-test

Figure 6E+F	Mean values of 15 samples per condition analyzed in four independent experiments	Standard error	ANOVA on ranks/ Tukey test
Figure 6G	Percent change values of four and three independent experiments for days 2 and 3, respectively	Standard error	Two-tailed unpaired t-test
Figure 6H	Percent change values of five and four independent experiments for days 2 and 3, respectively	Standard error	Rank Sum Test
Figure 6I	Percent change values of four independent experiments	Standard error	Rank Sum Test
Figure 6K	Mean values of four experiments done in parallel (in each case two performed with the acid and two with the hot ethanol extraction methods)	Standard error	Two-tailed unpaired t-test

Table S2 (related to Figure 5):

Protein alterations in crude mitochondrial extracts upon expression of UBB^{+1}

Protein alterations in crude mitochondrial extracts were determined with the quantitative SILAC approach in two independent experiments (this Table, and Tables S3, S4). Protein alterations upon expression of UBB^{+1} as compared with vector controls were shown here. n.D. no Data.

Protein ID	Gene Name	ORF Name	log_2 ratio UBB^{+1} *vs.* ctrl (Exp. 1)	Significance A (Exp. 1)	log_2 ratio UBB^{+1} *vs.* ctrl (Exp. 2)	Significance A (Exp. 2)	Description	Comigration with highly purified mitochondria
P50276	MUP1	YGR055W	-2.02	0.000000	-0.49	0.016303	High-affinity methionine permease	n.D.
P40088	FTR1	YER145C	-1.78	0.000011	-0.46	0.023565	Plasma membrane iron permease	n.D.
P39003; P23585	HXT6	YDR343C	-1.29	0.001672	-0.98	0.000002	High-affinity hexose transporter HXT6	(Prokisch et al., 2004; Reinders et al., 2006; Sickmann et al., 2003)
P32804	ZRT1	YGL255W	-1.23	0.002870	-0.72	0.000401	Zinc-regulated transporter 1	n.D.
P41807	VMA13	YPR036W	-0.88	0.039215	-0.43	0.033688	V-type proton ATPase subunit H	n.D.
P00549	CDC19	YAL038W	-0.86	0.045276	-0.60	0.003465	Pyruvate kinase 1	n.D.
P38998	LYS1	YIR034C	0.50	0.040053	0.63	0.012151	Saccharopine dehydrogenase [NAD(+), L-lysine-forming]	(Ohlmeier et al., 2004)
Q00055	GPD1	YDL022W	0.57	0.021970	0.97	0.000100	Glycerol-3-phosphate dehydrogenase [NAD(+)] 1	n.D.
Q01217	ARG5,6	YER069W	0.67	0.008110	0.78	0.001660	Protein ARG5,6, mitochondrial; N-acetyl-gamma-glutamyl-phosphate reductase; Acetylglutamate kinase	(Ohlmeier et al., 2004; Prokisch et al., 2004; Reinders et al., 2006; Sickmann et al., 2003)
P53101	STR3	YGL184C	0.73	0.004291	1.11	0.000008	Cystathionine beta-lyase	n.D.
P18544	ARG8	YOL140W	0.80	0.002093	0.66	0.008115	Acetylornithine aminotransferase, mitochondrial	(Ohlmeier et al., 2004; Prokisch et al., 2004; Reinders et al., 2006; Sickmann et al., 2003)
P36006	MYO3	YKL129C	0.85	0.001161	0.55	0.027030	Myosin-3	n.D.
P61830	HHT1	YBR010W	0.89	0.000703	1.07	0.000019	Histone H3	(Prokisch et al., 2004)
P04912; P04911	HTA2; HTA1	YBL003C; YDR225W	1.03	0.000109	0.51	0.041653	Histone H2A.2; Histone H2A.1	(Prokisch et al., 2004)
P02294; P02293	HTB2; HTB1	YBL003C; YDR224C	1.06	0.000072	0.54	0.030804	Histone H2B.2; Histone H2B.1	(Prokisch et al., 2004)
P09368	PUT1	YLR142W	3.46	0.000000	1.57	0.000000	Proline dehydrogenase, mitochondrial	(Reinders et al., 2006; Sickmann et al., 2003)

Table S3 (related to Figure 6):

Protein alterations in crude mitochondrial extracts upon expression of UBB^{+1} and increased levels of Vms1

Protein alterations in crude mitochondrial extracts were determined with the quantitative SILAC approach in two independent experiments (this Table, and Tables S2, S4). Protein alterations upon co-expression of UBB^{+1} and Vms1, *i.e.* elevated Vms1 levels, as compared with the single expression of UBB^{+1}, *i.e.* endogenous Vms1 levels, were shown here. Green-labeled proteins were inversely regulated as compared with Figure 5A/Table S2. n.D.: no Data.

Protein ID	Gene Name	ORF Name	log_2 ratio UBB^{+1} + Vms1 *vs.* UBB^{+1} (Exp. 1)	Significance A (Exp. 1)	log_2 ratio UBB^{+1} + Vms1 *vs.* UBB^{+1} (Exp. 2)	Significance A (Exp. 2)	Description	Comigration with highly purified mitochondria
P09368	PUT1	YLR142W	-2.24	0.000000	-1.48	0.000000	Proline dehydrogenase, mitochondrial	(Reinders et al., 2006; Sickmann et al., 2003)
P04912; P04911	HTA2; HTA1	YBL003C; YDR225W	-1.74	0.000000	-1.01	0.000000	Histone H2A.2; Histone H2A.1	(Prokisch et al., 2004)
P02294; P02293	HTB2; HTB1	YBL003C; YDR224C	-1.73	0.000000	-1.05	0.000000	Histone H2B.2; Histone H2B.1	(Prokisch et al., 2004)
P02309	HHF1	YBR009C	-1.66	0.000000	-1.09	0.000000	Histone H4	(Prokisch et al., 2004)
Q03940	RVB1	YDR190C	-1.48	0.000002	-0.50	0.003330	RuvB-like protein 1	(Ohlmeier et al., 2004)
P32451	BIO2	YGR286C	-1.11	0.000419	-1.55	0.000000	Biotin synthase, mitochondrial	(Prokisch et al., 2004)
P53101	STR3	YGL184C	-0.96	0.002306	-0.49	0.003858	Cystathionine beta-lyase	n.D.
P18544	ARG8	YOL140W	-0.78	0.012691	-0.83	0.000001	Acetylornithine aminotransferase, mitochondrial	(Ohlmeier et al., 2004; Prokisch et al., 2004; Reinders et al., 2006; Sickmann et al., 2003)
P32457	CDC3	YLR314C	-0.78	0.013275	-0.76	0.000009	Cell division control protein 3	n.D.
P38998	LYS1	YIR034C	-0.77	0.014649	-0.46	0.006765	Saccharopine dehydrogenase [NAD(+), L-lysine-forming]	(Ohlmeier et al., 2004)
P37291	SHM2	YLR058C	-0.74	0.017978	-0.72	0.000025	Serine hydroxymethyltransferase, cytosolic	(Ohlmeier et al., 2004)
P40531	GVP36	YIL041W	-0.74	0.019444	-0.48	0.004750	Protein GVP36	(Ohlmeier et al., 2004)
P53744	BIO5	YNR056C	-0.65	0.039746	-1.56	0.000000	7-keto 8-aminopelargonic acid transporter	n.D.
Q01217	ARG5,6	YER069W	-0.62	0.049814	-0.45	0.007580	Protein ARG5,6, mitochondrial; N-acetyl-gamma-glutamyl-phosphate reductase; Acetylglutamate kinase	(Ohlmeier et al., 2004; Prokisch et al., 2004; Reinders et al., 2006; Sickmann et al., 2003)
P21147	OLE1	YGL055W	0.40	0.047961	0.34	0.034115	Acyl-CoA desaturase 1	(Prokisch et al., 2004)
Q04182	PDR15	YDR406W	0.46	0.024889	0.73	0.000006	ATP-dependent permease PDR15	(Prokisch et al., 2004)
P39002	FAA3	YIL009W	0.55	0.007085	0.69	0.000016	Long-chain-fatty-acid--CoA ligase 3	n.D.
P05374	CHO2	YGR157W	0.63	0.002186	0.49	0.002201	Phosphatidylethanolamine N-methyltransferase	(Prokisch et al., 2004)
P38695	HXT5	YHR096C	0.65	0.001401	0.65	0.000058	Probable glucose transporter HXT5	n.D.
P32466	HXT3	YDR345C	0.69	0.000719	0.75	0.000003	Low-affinity glucose transporter HXT3	(Prokisch et al., 2004)

P39003; P23585	HXT6	YDR343C	0.72	0.000418	0.65	0.000058	High-affinity hexose transporter HXT6	(Prokisch et al., 2004; Reinders et al., 2006; Sickmann et al., 2003)
Q12252	PHM7	YOL084W	0.80	0.000102	0.86	0.000000	Phosphate metabolism protein 7	n.D.
P10614	ERG11	YHR007C	0.93	0.000007	0.60	0.000176	Lanosterol 14-alpha demethylase	(Prokisch et al., 2004)
P40088	FTR1	YER145C	1.02	0.000001	0.94	0.000000	Plasma membrane iron permease	n.D.
P50276	MUP1	YGR055W	1.04	0.000000	0.70	0.000014	High-affinity methionine permease	n.D.
P30605	ITR1	YDR497C	1.11	0.000000	0.36	0.026461	Myo-inositol transporter 1	n.D.
P19358; P10659	SAM2; SAM1	YDR502C; YLR180W	1.11	0.000000	0.37	0.021859	S-adenosylmethionine synthase 2; S-adenosylmethionine synthase 1	(Ohlmeier et al., 2004)
P48016	ATH1	YPR026W	1.21	0.000000	1.37	0.000000	Vacuolar acid trehalase	(Prokisch et al., 2004)
P38993	FET3	YMR058W	1.43	0.000000	0.86	0.000000	Iron transport multicopper oxidase FET3	n.D.
P32791	FRE1	YLR214W	1.96	0.000000	0.71	0.000010	Ferric/cupric reductase transmembrane component 1	n.D.
Q04311	VMS1	YDR049W	2.02	0.000000	3.29	0.000000	Protein VMS1	(Prokisch et al., 2004; Reinders et al., 2006; Sickmann et al., 2003)
P19657	PMA2	YPL036W	2.12	0.000000	0.50	0.001871	Plasma membrane ATPase 2	(Prokisch et al., 2004; Reinders et al., 2006; Sickmann et al., 2003)

Table S4 (related to Tables S2+S3):

Protein identifications and quantification by SILAC analysis of crude mitochondrial extracts

Protein alterations in crude mitochondrial extracts were determined with the quantitative SILAC approach in two independent experiments (this table, and Tables S2, S3). PEP: posterior error probability.

Protein ID	Gene Name	ORF Name	Peptides	Sequence Coverage	PEP
Q01217	ARG5,6	YER069W	39	49.9	0
P18544	ARG8	YOL140W	16	46.1	1.55E-88
P48016	ATH1	YPR026W	2	1.9	8.72E-05
P32451	BIO2	YGR286C	17	34.4	1.19E-72
P53744	BIO5	YNR056C	4	5.9	9..93E-09
P32457	CDC3	YLR314C	4	10.4	1.83E-13
P00549	CDC19	YAL038W	17	33.6	7.78E-76
P05374	CHO2	YGR157W	19	25.8	2.27E-191
P10614	ERG11	YHR007C	6	17.7	8.05E-44
P39002	FAA3	YIL009W	5	5.5	6.59E-10
P38993	FET3	YMR058W	5	14.2	1.40E-35
P32791	FRE1	YLR214W	4	7.9	1.24E-23
P40088	FTR1	YER145C	4	11.9	1.22E-38
Q00055	GPD1	YDL022W	3	10.2	4.56E-23
P40531	GVP36	YIL041W	2	6.4	1.72E-09
P02309	HHF1	YBR009C	5	54.4	4.66E-15
P61830	HHT1	YBR010W	2	11.8	9.71E-06
P04912;	HTA2;	YBL003C;	3	34.8	2.69E-08
P04911	HTA1	YDR225W			
P02294;	HTB2;	YBL003C;	4	26.0	6.67E-13
P02293	HTB1	YDR224C			
P32466	HXT3	YDR345C	6	10.1	9.23E-57
P38695	HXT5	YHR096C	15	25.7	2.91E-122
P39003;	HXT6	YDR343C	20	32.8	0
P23585					
P30605	ITR1	YDR497C	6	7.9	2.61E-98
P38998	LYS1	YIR034C	12	50.1	1.67E-123
P50276	MUP1	YGR055W	3	3.7	4.09E-12
P36006	MYO3	YKL129C	4	4.8	1.51E-16
P21147	OLE1	YGL055W	14	33.9	9.07E-60
Q04182	PDR15	YDR406W	2	1.6	2.29E-06
Q12252	PHM7	YOL084W	6	7.7	6.00E-17
P19657	PMA2	YPL036W	42	30.0	0
P09368	PUT1	YLR142W	4	9.7	3.04E-29
Q03940	RVB1	YDR190C	6	19.7	2.90E-41
P19358;	SAM2;	YDR502C;	3	7.3	1.14E-18
P10659	SAM1	YLR180W			
P37291	SHM2	YLR058C	18	40.3	1.57E-161
P53101	STR3	YGL184C	3	7.7	1.63E-52
P41807	VMA13	YPR036W	7	15.1	6.38E-48
Q04311	VMS1	YDR049W	26	40.0	4.19E-182
P32804	ZRT1	YGL255W	6	14.4	4.93E-34

Table S5 (related to Figure 7):

Immunoreactivities in the human hippocampus and entorhinal cortex for VMS1

Tissues were obtained from non-demented controls and AD patients. The neuropathological state was confirmed by the presence of β-amyloid plaques and neurofibrillary tangles (-: no, a: minor, b: moderate, c: strong staining). Immunohistochemistry for VMS1 using human paraffin sections (#) and a human Vibratome section (*). VMS1 staining of tangle-like structures was observed in 6 out of 11 non-demented controls (55%) but in 15 out of 20 AD patients (75%). 5 out of 6 non-demented controls with VMS1 staining of tangle-like structures were 72 years and older and these show both neurofibrillary tangles and UBB^{+1} accumulation. 13 out of 15 AD patients with VMS1 staining of tangle-like structures do show both neurofibrillary tangles and UBB^{+1} accumulation. [1]Information provided by the Netherlands Brain Bank.

Patient	Age (years)[1]	Sex (F/M)[1]	Plaques[1]	Tangles[1]	UBB^{+1} accumulation[1] ($Ubi2^{+1}$)	VMS1 staining of tangle-like structures
Non-demented controls						
01#	34	M	-	-	-	-
01#	43	M	-	-	-	-
03#	51	M	-	-	-	+++
04#	58	M	-	+[a]	+	-
05#	65	F	-	-	-	-
06#	72	M	+[b]	+[c]	+	+
07#	80	F	+[b]	+[c]	+	++
08#	82	F	-	+[c]	+	+
09#	85	M	+[b]	+[b]	+	+
10#	90	F	+[b]	+[b]	+	+
11#	90	F	-	+[a]	+	-
AD patients						
12#	40	M	+[a]	+[c]	+	+++
13#	49	M	+[b]	+[c]	+	+
14#	54	F	+[b]	+[c]	+	++
15#	56	F	+[b]	+[a]	-	++
16#	61	M	+[b]	+[c]	+	++
17#	66	M	+[c]	+[c]	+	-
18#	70	F	+[c]	+[a]	+	+
19#	70	M	+[c]	+[c]	-	-
20#	73	F	+[b]	+[c]	+	-
21#	77	M	+[b]	+[c]	+	+++
22#	77	M	+[b]	+[c]	-	+++
23#	81	M	+[b]	+[c]	+	+++
24#	83	F	+[b]	+[c]	+	++
25#	85	F	+[b]	+[c]	+	+
26#	86	M	+[b]	+[c]	+	++
27#	88	M	+[b]	+[c]	+	-
28#	90	F	+[c]	+[c]	+	-
29#	92	F	+[c]	+[c]	+	+++
30#	83	F	+[c]	+[c]	+	+++
31*	92	F	+[c]	+[c]	+	+

Table S6 (related to Figures 7+S7 and Table S5):

Clinico-pathological information of non-demented controls and AD patients

Information provided by the Netherlands Brain Bank.

Patient	Braak stage	Age (years)	Sex (F/M)	Dementia duration (years)	Postmortem delay (h)	Fixation duration (days)	Brain weight (g)	Cause of death
Non-demented controls								
01	0	34	M	-	<17	1124	1348	Empyema of pleura, fibrous pleuritis and fibrous pericarditis, AIDS
02	0	43	M	-	23	53	1260	Non-Hodgkin lymphoma
03	0	51	M	-	6	47	1518	Liposarcoma, ileus
04	0	58	M	-	24	1088	1797	Lung carcinoma, massive hemorrhage
05	0	65	F	-	24	403	1234	Pulmonary embolism
06	2	72	M	-	4	126	1330	Myocardial infarction, cardiogenic shock
07	2	80	F	-	36	65	1205	Cardiogenic shock
08	1	82	F	-	48	38	1100	Myocardial infarction, ventricular fibrillation
09	3	85	M	-	5	126	1050	Cardiac failure, myocardial infarction, coronary sclerosis, lung emphysema
10	3	90	F	-	2	48	1110	Postoperative infections
11	1	90	F	-	5	143	1040	Metabolic acidosis
AD patients								
12	5	40	M	5-6	3	28	1410	AD, cachexia
13	6	49	M	6	4	33	1426	AD, epilepsy
14	5	54	F	5	3	78	1055	AD, cachexia
15	4	56	F	4-5	22	48	1180	AD, bronchopneumonia, dehydration
16	6	61	M	3	6	30	1180	AD, fever
17	6	66	M	15	3	30	1270	AD, ischemic cerebral stroke, cachexia, sepsis
18	6	70	F	12	13	34	780	AD, status epilepticus
19	6	70	M	12	4	125	1325	AD, ileus, urinary tract infection
20	5	73	F	11	4	66	1106	AD, dehydration, circulation failure
21	5	77	M	7	4	75	1168	AD, pneumonia
22	2	77	M	>5	4	127	1095	AD, bronchial pneumonia
23	5	81	M	6	4	66	1088	AD, bacterial infection
24	5	83	F	14	6	127	1005	AD, cachexia, urinary tract infection
25	4	85	F	4	2	39	1020	AD, heart disease, anaemia
26	5	86	M	10	4	77	1303	AD, uraemia
27	3	88	M	4	5	75	1058	AD, decompensatio cordis
28	5	90	F	>8	3	38	1060	AD, dehydration
29	4	92	F	3	4	124	896	AD, cachexia, uraemia
30	4	83	F	5	5	32.	1288	AD, vascular encephalopathy
31	5	92	F	6	3	335	964	AD, dehydration, cachexia

Supplemental Discussion

Here, we established a yeast model for dissecting cell death mechanisms triggered by UBB^{+1}. UBB^{+1} accumulation resulted in a progressive loss of clonogenic cell survival, accompanied with increased levels of oxidative stress, culminating in apoptosis and necrosis. In neuronal cultures, UBB^{+1} expression has been linked to apoptosis (de Vrij et al., 2001; Tan et al., 2007). However, either high expression levels or the presence of other neurotoxic proteins, such as huntingtin, were needed for efficient cell killing (de Pril et al., 2004; de Pril et al., 2007; de Pril et al., 2010; de Vrij et al., 2001; Tan et al., 2007). Consistently, transgenic expression of UBB^{+1} in mice failed to cause overt neurodegeneration although it did affect spatial reference memory and caused a central dysfunction of respiratory regulation (Fischer et al., 2009; Irmler et al., 2012; van Tijn et al., 2011). Therefore, our data support the hypothesis that prolonged high levels of UBB^{+1} are required for cell killing.

Several lines of evidence suggest for a pivotal role of mitochondria. Yeast cells expressing UBB^{+1} demonstrated (i) increased levels of oxidative stress, (ii) impaired recovery of the mitochondrial network, when shifting stationary yeast cultures to fresh media, (iii) increased cellular oxygen consumption, (iv) increased mitochondrial membrane potential, accompanied by (v) depletion of cellular ATP levels, and (vi) decrease in the mitochondrial respiratory chain components Rip1 and cytochrome *c*, and (vii) significantly attenuated cytotoxicity in a yeast strain lacking the second isoform of cytochrome *c*. Previously, it was shown that UBB^{+1} could trigger neuronal apoptosis accompanied by reduced mitochondrial movement (Tan et al., 2007). Mitochondrial impairment is an AD hallmark and likely contributes to neurodegeneration (Rodolfo et al., 2010). Therefore, the data obtained with UBB^{+1}-expressing yeast cells corroborate essential features of cell death-relevant mitochondrion dysfunctions found in AD neurons.

It appears intriguing that UBB^{+1} interferes with the UPS (Fischer et al., 2009; Lindsten et al., 2002; Tank and True, 2009; van Tijn et al., 2007; van Tijn et al., 2010) paralleling the

observation that the UPS is also compromised during aging and age-related neurodegeneration (Dennissen et al., 2010). In contrast, increased UPS capacities antagonize aging and increase life span in yeast and flies (Chondrogianni et al., 2014; Kruegel et al., 2011). Our data suggest that the cumulated impact of UBB^{+1} and the age-intrinsic derangement of the UPS contribute to the pathogenesis of AD and other UBB^{+1}-related disorders, implying that stimulation of the UPS might have neuroprotective effects.

Supplemental Experimental Procedures

Yeast expression plasmids

Construct name	Copy no.	Promoter	Plasmid selection	References
pESC-HIS-nFLAG	2µ	*GAL10*	HIS3	U. Janschek, University of Graz, Graz, Austria
pESC-HIS-nFLAG-UBB	2µ	*GAL10*	HIS3	This study
pESC-HIS-nFLAG-UBB^{+1}	2µ	*GAL10*	HIS3	This study
pESC-HIS-nFLAG-UBB^{+1}-K29,48R	2µ	*GAL10*	HIS3	This study
pESC-HIS	2µ	*GAL10*	HIS3	Agilent Technologies
pESC-HIS-TDP-43	2µ	*GAL10*	HIS3	(Braun et al., 2011)
pESC-HIS-Vms1	2µ	*GAL10*	HIS3	This study
pESC-LEU	2µ	*GAL10*	LEU2	Agilent Technologies
pESC-LEU-nFLAG-UBB^{+1}	2µ	*GAL10*	LEU2	This study
pYES2-mtyeRFP	2µ	*GAL1*	URA3	D. Scholz, University of Bayreuth, Bayreuth, Germany
pYES2-Ub-G76V-GFP	2µ	*GAL1*	URA3	(Heessen et al., 2003)
pBY011	ARS/CEN4	*GAL1*	URA3	PlasmID, DF/HCC DNA Resource Core, Boston, MA, USA
pBY011-RPN4	ARS/CEN4	*GAL1*	URA3	PlasmID
pRS426	2µ	*None*	URA3	Agilent Technologies
pRS426-Vms1	2µ	*Endogenous*	URA3	(Heo et al., 2010)

Using a PCR-based method, human ubiquitin B (UBB), frameshift UBB^{+1}, and UBB^{+1}-K29,48R were subcloned from pcDNA3.1 (van Tijn et al., 2007) via *Not*I and *Cla*I restriction sites into the multiple cloning site 1 of a modified pESC-HIS vector (Agilent Technologies, Waldbronn, Germany) encoding a human Kozak sequence and a N-terminal FLAG-tag. For this purpose, the following primers were designed (forward: 5'- AAT AGC GGC CGC CAT GCA GAT CTT CGT GAA AAC CCT TAC C-3' for UBB, UBB^{+1}, and UBB^{+1}-K29,48R) and (reverse: 5'-TTA TAT CGA TTC ACT GGG CTC CAC TTC CAG GG-3' for UBB^{+1}, and UBB^{+1}-K29,48R; reverse: 5'-TAT TAT CGA TTC AAC CAC CTC TCA GAC GCA GGA CCA GGT G-3' for UBB).

Yeast strains and growth conditions

Yeast strain	Strain type	Genetic background	References
BYa wt	BY4741	MATa, *his3*Δ1; *leu2*Δ0; *met15*Δ0; *ura3*Δ0; ρ^+	EUROSCARF
BYa wt ρ^0	BY4741	MATa, *his3*Δ1; *leu2*Δ0; *met15*Δ0; *ura3*Δ0; ρ^0	(Büttner et al., 2008)
BYa Δ*aif1*	BY4741	MATa, *his3*Δ1; *leu2*Δ0; *met15*Δ0; *ura3*Δ0; *YNR074C*::kanMX4	EUROSCARF
BYa Δ*arg1*	BY4741	MATa, *his3*Δ1; *leu2*Δ0; *met15*Δ0; *ura3*Δ0; *YOL058W*::kanMX4	EUROSCARF
BYa Δ*arg2*	BY4741	MATa, *his3*Δ1; *leu2*Δ0; *met15*Δ0; *ura3*Δ0; *YJL071W*::kanMX4	EUROSCARF
BYa Δ*arg3*	BY4741	MATa, *his3*Δ1; *leu2*Δ0; *met15*Δ0; *ura3*Δ0; *YJL088W*::kanMX4	EUROSCARF
BYa Δ*arg4*	BY4741	MATa, *his3*Δ1; *leu2*Δ0; *met15*Δ0; *ura3*Δ0; *YHR018C*::kanMX4	EUROSCARF
BYa Δ*arg4* Δ*lys2* (for SILAC and targeted metabolomics)	BY4741	MATa, *his3*Δ1; *leu2*Δ0; *met15*Δ0; *ura3*Δ0; *YHR018C*::kanMX4; *YBR115C*::*URA3*	(Büttner et al., 2013)
BYa Δ*arg5,6*	BY4741	MATa, *his3*Δ1; *leu2*Δ0; *met15*Δ0; *ura3*Δ0; *YER069W*::kanMX4	EUROSCARF
BYa Δ*arg7*	BY4741	MATa, *his3*Δ1; *leu2*Δ0; *met15*Δ0; *ura3*Δ0; *YMR062C*::kanMX4	EUROSCARF
BYa Δ*arg8*	BY4741	MATa, *his3*Δ1; *leu2*Δ0; *met15*Δ0; *ura3*Δ0; *YOL140W*::kanMX4	Open Biosystems
BYa Δ*cyc1*	BY4741	MATa, *his3*Δ1; *leu2*Δ0; *met15*Δ0; *ura3*Δ0; *YJR048W*::kanMX4	EUROSCARF
BYa Δ*cyc7*	BY4741	MATa, *his3*Δ1; *leu2*Δ0; *met15*Δ0; *ura3*Δ0; *YEL039C*::kanMX4	EUROSCARF
BYa Δ*gpd1*	BY4741	MATa, *his3*Δ1; *leu2*Δ0; *met15*Δ0; *ura3*Δ0; *YDL022W*::kanMX4	Open Biosystems
BYa Δ*hac1*	BY4741	MATa, *his3*Δ1; *leu2*Δ0; *met15*Δ0; *ura3*Δ0; *YFL031W*::kanMX4	EUROSCARF
BYa Δ*ire1*	BY4741	MATa, *his3*Δ1; *leu2*Δ0; *met15*Δ0; *ura3*Δ0; *YHR079C*::kanMX4	EUROSCARF
BYa Δ*kex1*	BY4741	MATa, *his3*Δ1; *leu2*Δ0; *met15*Δ0; *ura3*Δ0; *YGL203C*::kanMX4	EUROSCARF
BYa Δ*lys1*	BY4741	MATa, *his3*Δ1; *leu2*Δ0; *met15*Δ0; *ura3*Δ0; *YIR034C*::kanMX4	EUROSCARF
BYa Δ*myo3*	BY4741	MATa, *his3*Δ1; *leu2*Δ0; *met15*Δ0; *ura3*Δ0; *YKL129C*::kanMX4	Open Biosystems
BYa Δ*npl4*	BY4741	MATa, *his3*Δ1; *leu2*Δ0; *met15*Δ0; *ura3*Δ0; *YBR170C*::kanMX4	EUROSCARF
BYa Δ*nuc1*	BY4741	MATa, *his3*Δ1; *leu2*Δ0; *met15*Δ0; *ura3*Δ0; *YJL208C*::kanMX4	EUROSCARF
BYa Δ*ort1*	BY4741	MATa, *his3*Δ1; *leu2*Δ0; *met15*Δ0; *ura3*Δ0; *YOR130C*::kanMX4	EUROSCARF
BYa Δ*put1*	BY4741	MATa, *his3*Δ1; *leu2*Δ0; *met15*Δ0; *ura3*Δ0; *YLR142W*::kanMX4	Open Biosystems
BYa Δ*rpn4*	BY4741	MATa, *his3*Δ1; *leu2*Δ0; *met15*Δ0; *ura3*Δ0; *YDL020C*::kanMX4	EUROSCARF
BYa Δ*str3*	BY4741	MATa, *his3*Δ1; *leu2*Δ0; *met15*Δ0; *ura3*Δ0; *YGL184C*::kanMX4	Open Biosystems
BYa Δ*ubi4*	BY4741	MATa, *his3*Δ1; *leu2*Δ0; *met15*Δ0; *ura3*Δ0; *YLL039C*::kanMX4	EUROSCARF
BYa Δ*ubp6*	BY4741	(yMS485) MATa *his3*Δ1; *leu2*Δ0; *met15*Δ0; *ura3*Δ0; *ubp6*Δ::*URA3*	(Kruegel et al., 2011)
BYa Δ*ubr2*	BY4741	(BR2194) MATα *his3*Δ1; *leu2*Δ0; *met15*Δ0; *ura3*Δ0; *ubr2*Δ::*URA3*	(Kruegel et al., 2011)

BYa Δ*vms1*	BY4741	MATa, *his3*Δ1; *leu2*Δ0; *met15*Δ0; *ura3*Δ0; *YDR049W*::kanMX4	(Heo et al., 2010)
BYa Δ*ybh3*	BY4741	MATa, *his3*Δ1; *leu2*Δ0; *met15*Δ0; *ura3*Δ0; *YNL305C*::kanMX4	EUROSCARF
BYa Δ*yuh1*	BY4741	MATa, *his3*Δ1; *leu2*Δ0; *met15*Δ0; *ura3*Δ0; *YJR099W*::kanMX4	Open Biosystems
WCG4a wt	WCG4a	MATa; *ura3*; *leu2-3,112*; *his3-11,15*; Can^S Gal^+	(Heinemeyer et al., 1993)
WCG4a *pre1-1*	WCG4a	MATa; *pre1-1*; *ura3*; *leu2-3,112*; *his3-11,15*; Can^S Gal^+	(Heinemeyer et al., 1993)
WCG4a *pre2-1*	WCG4a	MATa; *pre2-1*; *ura3*; *leu2-3,112*; *his3-11,15*; Can^S Gal^+	(Heinemeyer et al., 1993)
WCG4a *pre2-2*	WCG4a	MATa; *pre2-2*; *ura3*; *leu2-3,112*; *his3-11,15*; Can^S Gal^+	(Heinemeyer et al., 1993)
WCG4a *pre1-1 pre2-1*	WCG4a	MATa; *pre1-1*; *pre2-1*; *ura3*; *leu2-3,112*; *his3-11,15*; Can^S Gal^+	(Heinemeyer et al., 1993)
WCG4a *pre1-1 pre2-2*	WCG4a	MATa; *pre1-1*; *pre2-2*; *ura3*; *leu2-3,112*; *his3-11,15*; Can^S Gal^+	(Heinemeyer et al., 1993)
WCG4a *CDC48*-wt	WCG4a	MATa; *ura3*; *leu2-3,112*; *his3-11,15*; *cdc48::URA3*; YEp52(*LEU2*)-*CDC48*	(Jarosch et al., 2002)
WCG4a *cdc48*-S565G	WCG4a	MATa; *ura3*; *leu2-3,112*; *his3-11,15*; *cdc48::URA3*; YEp52(*LEU2*)-*cdc48*-S565G	(Jarosch et al., 2002)
CEN.PK-113-7D (for generation of internal standards for targeted metabolomics)			M. Klimacek, TU Graz, Graz, Austria

Strains were grown in YPD according to (Sherman, 2002), or in synthetic complete (SC) media either according to (Sherman, 2002) or containing 0.17% yeast nitrogen base (Difco, Otto Nordwald, Hamburg, Germany), 0.5% $(NH_4)_2SO_4$ and 30 mg/L of all amino acids (except 80 mg/L histidine and 200 mg/L leucine), 30 mg/L adenine, and 320 mg/L uracil. SC media contained either 2% glucose (SCD) or 2% galactose (SCGal) as carbon sources. Plasmid transformation and maintenance were done by growth in selective SC media, using the auxotrophic markers of the yeast strains. Gene expression was under the control of galactose-regulated promoters. Transformed yeast strains were pre-grown in selective SC media repressing expression (SCD) for 6 h at 28°C in either flasks with 145 rpm or in 96 deep-wells with 250 rpm until an OD_{600} of 0.4. Expression was induced either in quadruple-indented flasks or in 96 deep-wells by shifting to selective SC media inducing expression (SCGal).

For stable isotope labeling (SILAC) and targeted metabolomics, a yeast strain of BY4741 background lacking *ARG4* and *LYS2* genes was co-transformed with either two vector controls (pESC-LEU-nFLAG and pESC-HIS), or with UBB^{+1} expression construct and

vector control (pESC-LEU-nFLAG-UBB^{+1} and pESC-HIS), or with both UBB^{+1} and Vms1 expression constructs (pESC-LEU-nFLAG-UBB^{+1} and pESC-HIS-Vms1). Yeast cells were grown in SC media according to (Sherman, 2002) with the following modifications: 30 mg/L proline, 50 mg/L arginine, 80 mg/L lysine. For SILAC, yeast cells were grown in media supplemented either with Lys0 and Arg0 (normal isotopes), or with Lys4 and Arg6, or with Lys8 and Arg10 (heavy isotopes, Silantes, Munich, Germany). In a biological replicate the assignment of the isotope labels was changed. Pre-growth in SCD media and expression in SCGal media was done as described above. For targeted metabolomics, yeast cells were grown in media supplemented with Lys0 and Arg0 (normal isotopes).

Determination of respiratory deficiency

Wild-type and knock-out strains were streaked out on YPD (4% glucose, 1% yeast extract, 2% bacto peptone, 2% Agar; Difco) and YPGly (3% glycerol, 1% yeast extract, 2% bacto peptone, 2% Agar Agar). Plates were incubated at 30°C for three days. Respiratory deficiency of the respective yeast strains was indicated by a growth deficiency on YPGly, which can only be used to support growth by respiration.

Measuring cytotoxicity based on growth

Yeast clones transformed with UBB^{+1} and TDP-43 constructs or vector controls were grown overnight in SCD-HIS medium. For spot dilution assays (growth on solid media), cultures were normalized to an optical density (OD_{600}) of 0.5 in ddH_2O, serially diluted (1:10) in ddH_2O, and spotted onto solid nutrient-containing media inducing (SCGal-HIS) or repressing (SCD-HIS) expression of UBB^{+1} or TDP-43. Plates were incubated for two days at 30°C before analysis. For growth assays (growth in liquid media), cultures were diluted in SCD-HIS media and grown to an OD_{600} of 0.4, shifted to expression medium (SCGal-HIS), and grown overnight. After dilution in expression medium to an OD_{600} of 0.1 growth was

followed at 30°C in quadruple-indented flasks. Three samples (*i.e.* three distinct yeast clones per transformed construct) were measured in parallel. The mean values and the standard deviations were calculated from the OD_{600} values of the samples and illustrated graphically (see Figures 2B).

Measuring cytotoxicity based on clonogenicity/survival

Clonogenic assays determine the survivability of yeast cultures by determining the number of yeast cells that remain capable to form new colonies on agar plates upon ideal nutrient conditions. Cell densities (cells/mL) of yeast cultures expressing proteins or carrying vector controls were measured with an automated cell counter (CASY1, Roche Innovatis, Bielefeld, Germany, or Z2 Coulter Particle Count and Size Analyzer, Beckman Coulter, Krefeld, Germany). For this, (stationary) cultures were diluted in PBS (1:1,000), and the number of cells (particles with the size of 2 to 6.7 µm) was determined by measuring voltage variations during vacuuming of 100 µL aliquots through a 50 µM aperture. Each sample measurement was performed in duplicate. For plating, cultures were diluted in ddH_2O, and aliquots containing 500 cells were plated either on YPD or on selective SC agar plates containing glucose, on which expression of proteins of interest was repressed. The colony forming units (CFUs), *i.e.*, colonies grown after two days of incubation at 30°C were counted manually, or automatically using a colony counter (LemnaTech, Würselen, Germany).

In every experiment and for every time point or condition (*e.g.* stressed *vs.* unstressed), the CFU of a culture inoculated by an individual yeast clone was determined in duplicate. At least three distinct yeast clones per yeast strain and transformed construct were analyzed in parallel. In other words, in every experiment and for every time point or condition, the CFU of a distinct yeast strain transformed with a distinct construct was based on at least six CFU measurements. Further, each experiment was repeated independently for at least three times.

The mean values and the standard errors were calculated from the CFUs of all experiments and illustrated graphically (see Figures 2C, S2A+B). For statistical analysis, the absolute clonogenicities (CFU[500]) of the different strains were compared.

When comparing the cytotoxic effects of UBB^{+1} in different yeast strains, the CFUs obtained using yeast cells carrying vector controls were set to 100% in every experiment and strain. The mean values and the standard errors were calculated from the relative clonogenicities of all experiments and illustrated graphically as percent change values (Survival [%]) (see Figures 3B+D, 4H+I, 5B, 6A-C, Figures S3A+B, S4D+E, S5A, S6A-C). For statistical analysis the relative clonogenicities upon UBB^{+1} expression among the different strains (usually wild-type *vs.* mutant strains) were compared.

When comparing the protective effects of Rpn4 or Vms1 in cells expressing UBB^{+1}, the CFUs obtained using yeast cells without UBB^{+1} expression were set to 100% in every experiment and strain. The mean values and the standard errors were calculated from the relative clonogenicities of all experiments and illustrated graphically as percent change values (Survival upon UBB^{+1} expression [%]) (see Figures 3F, 6D, Figures S3C, S6D). For statistical analysis the relative clonogenicities upon UBB^{+1} expression between strains with endogenous levels of Rpn4 or Vms1, or elevated levels of Rpn4 or Vms1 were compared.

Measurement of oxidative stress and cell death

Oxidative stress was determined by measuring the conversion of dihydroethidium (DHE, Sigma-Aldrich, Vienna, Austria) to the red fluorescent ethidium (Madeo et al., 1999) applying a fluorescence plate reader. $5x10^6$ cells per sample were pelleted in 96-well plates. Cell pellets in each well were resuspended in 250 µL DHE-staining solution (2.5 µg/mL in PBS for DHE; 2.5 mg/mL DHE stock solution in DMSO). After 10 min of incubation at RT, fluorescence was measured as relative fluorescence units (RFU) in the GENiosPro 96-well fluorescence plate reader (Tecan, Grödig, Austria) with the following settings: fluorescence

top, excitation 515 nm, emission 595 nm, gain 45, number of reads 6, integration time 40 µs. Staining solution was used for blank measurements. Samples were measured in duplicate, and at least three samples (*i.e.* distinct yeast clones) were determined per strain, construct, and condition. Experiments were repeated independently at least five times. The mean values and the standard errors were calculated from the RFUs of all experiments and illustrated graphically (see Figures 2D, S2A+B). For statistical analysis, the RFUs of the different strains were compared.

For validating data on an individual cell basis, DHE- or PI-stained samples (propidium iodide [PI] is a 'vital dye', which stains cells with disintegrated plasma membranes) were measured by flow cytometry (BD FACSAria, BD Biosciences, Heidelberg, Germany) with the following settings: filter sets: PE for DHE (excitation 488/532 nm, emission 578 nm) and PerCP-Cy5.5 for PI (excitation, 488/532 nm, emission, 695 nm); flow rate: 4. Results were analyzed with the BD FACSDiva software V 5.0. 30,000 cells were evaluated per sample, and at least three samples (*i.e.* distinct yeast clones) were determined per strain, construct, and condition. Unstained samples were used as controls. Experiments were repeated independently at least four times. The mean values and the standard errors were calculated from the proportions of stained cells (%) of all experiments and illustrated graphically (see Figures 4A, 6E+F). For statistical analysis, the proportions of stained cells (%) of the different strains were compared.

For measuring oxidative stress levels (DHE) and incidences of cell death (PI) upon UBB^{+1} expression in strains with disrupted arginine/ornithine or lysine biosynthesis the subsequent analysis was performed by flow cytometry (BD LSRFortessa, BD Biosciences) as described above. 30,000 cells per sample were evaluated by using BD FACSDiva software (BD Biosciences). Six samples (*i.e.* distinct yeast clones) were determined per strain, construct, and condition. Experiments were repeated independently at least three times. When comparing the cytotoxic effects of UBB^{+1} in different yeast strains, the proportions of DHE-

or PI-stained cells obtained using yeast cells carrying vector controls were set to 100% in every experiment, strain, and condition. The mean values and the standard errors were calculated from the relative DHE- or PI-staining of all experiments and illustrated graphically as percent change values (DHE -> Ethidium [%] or PI staining [%]) (see Figures 5E-G, Figures S5B). For statistical analysis the relative DHE- or PI-staining upon UBB^{+1} expression among the different strains (usually wild-type *vs.* mutant strains) were compared.

Determination of morphological markers of apoptosis and necrosis

Annexin V/PI co-staining (with Annexin V-FLUOS Staining Kit, Roche Applied Sciences, Mannheim, Germany, and PI, Sigma-Aldrich) and terminal deoxynucleotidyl transferase dUTP nick end labeling (TUNEL) (*In Situ* Cell Death Detection Kit, Roche Applied Sciences) were performed to discriminate among early apoptotic, late apoptotic/secondary necrotic and necrotic cells, or between apoptotic and non-apoptotic cells, respectively (Büttner et al., 2007). To determine the frequency of morphological phenotypes, cells were evaluated by flow cytometry (BD FACSAria) and BD FACSDiva software V 5.0 with the following settings: for Annexin V/PI: filter sets FITC (excitation 488 nm, emission 519 nm) and PerCP-Cy 5.5 (excitation 488/532 nm, emission 695 nm), flow rate: 1; for TUNEL: filter set FITC (excitation 488 nm, emission 519 nm); spectral overlap PerCP-Cy 5.5/FITC: 4.0; flow rate: 1. 30,000 cells were evaluated per sample, and at least three samples (*i.e.* distinct yeast clones) were determined per strain, construct, and condition. Unstained samples and PI-only and Annexin V-only stained samples were used as controls. Experiments were performed independently eight times. The mean values and the standard errors were calculated from the proportions of stained cells (%) of all experiments and illustrated graphically (see Figures 2E+F). For statistical analysis, the proportions of stained cells (%) of the different strains were compared.

Measurement of mitochondrial fragmentation

UBB^{+1} or vector control and a red fluorescent protein (yeRFP) fused with a mitochondrial targeting sequence (pYES2-mtyeRFP) were expressed (SCGal-URA/-HIS) for two days. Under these late stationary-phase conditions, the mitochondria were predominantly fragmented. In contrast to logarithmically growing cells, in which mitochondria are highly fused (Westermann, 2010). The two days old stationary phase cultures were then shifted to fresh media repressing expression of UBB^{+1} (SCD-URA/-HIS) and inducing regrowth of yeast cells. After 3 h the proportion of cells whose mitochondria remain fragmented was quantified. At least 500 cells were evaluated per experiment and condition. Experiments were repeated independently twelve times. Representative cells which expressed UBB^{+1} and mitochondrially-targeted yeRFP showing mitochondrial network and fragmented mitochondria, respectively, are shown in Figure S4A.

Measurement of cellular oxygen consumption

Oxygen consumption of stationary yeast cultures was analyzed using the FireSting optical oxygen sensor system (Pyro Science, Aachen, Germany). Prior to measurements the electrodes were calibrated with deionized H_2O representing the 100% reference value and 1% $NaSO_3$ representing 0% reference value. Oxygen depletion in 2 mL yeast culture samples was determined under continuous stirring at 28°C in 2 mL bottles, sealed with parafilm in order to avoid re-oxygenation of the medium. The decrease of the oxygen concentration over time was calculated and normalized to the number of living cells within the sample. The number of living cells was determined by measuring both the exact cell densities (cells/mL) using an automated cell counter (*e.g.* CASY1) and the proportion of these cells with intact plasma membrane (cells that are not stained with PI) using flow cytometry. At least four different samples (*i.e.* distinct yeast clones) were determined per strain, construct, and condition. Experiments were performed independently at least three times.

When analyzing the effects of UBB^{+1} expression on cellular oxygen consumption, the oxygen consumption of yeast cells carrying vector controls was set to 100% in every experiment. The mean values and the standard errors were calculated from the relative oxygen consumption of all experiments and illustrated graphically as percent change values (Cellular oxygen consumption [%]) (see Figure 4C). For statistical analysis the relative oxygen consumption upon UBB^{+1} expression was compared with the relative oxygen consumption of cells carrying vector controls.

When analyzing the effects of high Vms1 levels on cellular oxygen consumption of UBB^{+1}-expressing cells, the oxygen consumption of yeast cells with endogenous Vms1 levels was set to 100% in every experiment. The mean values and the standard errors were calculated from the relative oxygen consumption of all experiments and illustrated graphically as percent change values (Cellular oxygen consumption upon UBB^{+1} expression [%]) (see Figure 6G). For statistical analysis the relative oxygen consumption upon high levels of Vms1 (Vms1) expression was compared with the relative oxygen consumption of cells with endogenous levels of Vms1 (vector control).

Determination of mitochondrial membrane potential

Mitochondrial membrane potential was assessed cytofluorometrically by staining cells with tetramethylrhodamine methyl ester (TMRM, Molecular Probes, Life Technologies), a fluorescent dye that accumulates within mitochondria dependent on their membrane potential. Staining and analyses were performed as described in (Büttner et al., 2011) with slight modifications. Briefly, aliquots of $5x10^6$ cells were harvested at the indicated time points, washed and incubated with 5 µM TMRM at 28°C in the dark for 30 min. Cells were washed to remove excess dye and subjected to flow cytometric analyses using the BD LSRFortessa (BD Biosciences) with the following settings: filter sets: PE (excitation 488/532 nm, emission 578 nm); flow rate: 4. The mean fluorescence intensity of 30,000 cells per sample was

determined by subtracting the background signal of unstained samples. Data were normalized to the number of living cells within a sample as described in the 'measurement of cellular oxygen consumption'. At least four samples (*i.e.* distinct yeast clones) were measured per strain, construct, and condition. Experiments were performed independently at least four times.

When analyzing the effects of UBB^{+1} expression on mitochondrial membrane potential, the mitochondrial membrane potential of yeast cells carrying vector controls was set to 100% in every experiment. The mean values and the standard errors were calculated from the relative mitochondrial membrane potential of all experiments and illustrated graphically as percent change values (Mitochondrial membrane potential [%]) (see Figure 4D). For statistical analysis the relative mitochondrial membrane potential upon UBB^{+1} expression was compared with the relative mitochondrial membrane potential of cells carrying vector controls.

When analyzing the effects of Vms1 expression on mitochondrial membrane potential of UBB^{+1}-expressing cells, the mitochondrial membrane potential of yeast cells without Vms1 expression was set to 100% in every experiment. The mean values and the standard errors were calculated from the relative mitochondrial membrane potential of all experiments and illustrated graphically as percent change values (Mitochondrial membrane potential upon UBB^{+1} expression [%]) (see Figure 6H). For statistical analysis the relative mitochondrial membrane potential upon high levels of Vms1 (Vms1) was compared with the relative mitochondrial membrane potential of cells with endogenous levels of Vms1 (vector control).

Determination of cellular ATP level

To determine the ATP level of yeast cells, intracellular metabolites were obtained using hot ethanol extraction. Briefly, $1x10^8$ cells were harvested and quick-frozen in liquid nitrogen, resuspended in 0.5 mL of boiling ethanol (75% ethanol, 10 mM $(NH_4)_2SO_4$) and

incubated at 90°C for 3 min. Residual cell debris was removed by centrifugation (-4°C, 14,000 rpm, 20 min) and 10 µL of the supernatant was taken for the subsequent determination of ATP levels using the ATP Determination Kit (Molecular Probes, Life Technologies). This assay is based on an ATP-dependent reaction of recombinant firefly luciferase, which induces bioluminescence of its substrate D-luciferin and is directly correlated with the ATP content. Luminescence induced by the sample was assessed with a Luminoskan Ascent microplate reader (Labsystems, Thermo Scientific). Data were normalized to the number of living cells within a sample as described in the 'measurement of cellular oxygen consumption'. At least three samples (*i.e.* distinct yeast clones) were measured per strain, construct, and condition. Experiments were performed independently at least four times.

When analyzing the effects of UBB^{+1} expression on cellular ATP levels, the cellular ATP levels of yeast cells carrying vector controls was set to 100% in every experiment. The mean values and the standard errors were calculated from the relative cellular ATP levels of all experiments and illustrated graphically as percent change values (Cellular ATP level [%]) (see Figure 4E). For statistical analysis the relative cellular ATP levels upon UBB^{+1} expression was compared with the relative cellular ATP levels of cells carrying vector controls.

When analyzing the effects of Vms1 expression on cellular ATP levels of UBB^{+1}-expressing cells, the cellular ATP levels of yeast cells without Vms1 expression was set to 100% in every experiment. The mean values and the standard errors were calculated from the relative cellular ATP levels of all experiments and illustrated graphically as percent change values (Cellular ATP levels upon UBB^{+1} expression [%]) (see Figure 6I). For statistical analysis the relative cellular ATP levels upon high levels of Vms1 (Vms1) was compared with the relative cellular ATP levels of cells with endogenous levels of Vms1 (vector control).

Measurement of UPS activities

For determining the level of polyubiquitylated proteins in cellular extracts, immunoblots of cellular extracts were incubated with an ubiquitin-specific antibody (1:8000, mouse monoclonal, BD Biosciences). Immunosignals of the peak chain in the range of 15 to 200 kDa were quantified with ImageJ 1.47m as described in 'SDS-PAGE and immunoblot analyses'. The ubiquitin-specific immunosignals of the peak chain in the immunoblot lane which was loaded with extracts from cells transformed with vector controls were set to 100% in every experiment. The experiments were repeated independently for five times.

The ubiquitin-fusion protein ubiquitin-G76V-GFP was co-expressed with UBB^{+1} or vector controls in SCGal-HIS/-URA. GFP fluorescence (relative fluorescence units, RFU) and optical densities (OD_{600}) were determined in 96-well format using the FLUOstar Omega plate reader with the following settings for (i) OD_{600} measurements: number of flashes per scan point 5, path length correction 200 µL, well scanning 5x5, diameter 2 mm; for (ii) measurements of fluorescence intensities: endpoint, number of flashes per well 10, top optic, excitation 485 nm, emission 520 nm, gain 2000, orbital averaging 'on', diameter 2 mm. RFU was normalized to OD_{600} in every single well, in order to determine the level of ubiquitin-GFP fusion proteins per culture. Each sample was measured once. Five samples (*i.e.*, distinct yeast clones) were tested per construct, and condition. Experiments were performed independently at least five times. The mean values and the standard errors were calculated from the RFU/OD_{600} values of all experiments and illustrated graphically (see Figures 1D). For statistical analysis, the RFU/OD_{600} values of the different strains were compared.

Measurement of chymotrypsin-like proteasomal activities were performed using the Proteasome-Glo™ Cell-Based Assay (Promega, Heidelberg, Germany) (Ruenwai et al., 2011). Yeast strains with mutated genes encoding proteasomal subunits were grown in YPD until logarithmic phase, whereas cells expressing UBB^{+1} or *RPN4* were grown in SCGal-HIS or SCGal-URA for different periods. Cells were then diluted in YPD, and SCGal-HIS or

SCGal-URA, respectively, to an OD_{600} of 0.04 (equivalent to approximately 40'000 cells). 25 µL of diluted yeast cultures were then mixed with 25 µL of cell-based reagent. This reagent causes permeabilization of yeast cells, and enables the incorporation of the substrate succinyl-leucine-leucine-valine-tyrosine-aminoluciferin, which is specific for chymotrypsin-like proteasomal activities. The increase in luminescence activity (relative luminescence unit, RLU) by proteolytic cleavage of aminoluciferin was measured until steady state in 384-well format using the FLUOstar Omega plate reader (BMG Labtech, Ortenberg, Germany) with the following settings: measurement type luminescence, measurement interval time 5 sec, emission lens, gain 3600. Each sample was measured in triplicate. For UBB^{+1}, and *RPN4*-expressing cultures, at least three samples (*i.e.*, yeast clones transformed with expression constructs and vector controls, respectively) were tested per strain, construct, and condition. Experiments were performed independently at least three times. The RLUs obtained using yeast cells carrying vector controls (for Figures 3E and S1C) or wild-type yeast cells (for Figure 3A+C) were set to 100% in every experiment. The mean values and the standard errors were calculated from the relative proteasomal activities of all experiments and illustrated graphically as percent change values (Proteasomal activity [%]) (see Figure 3A+C+E, Figure S1C). For statistical analysis the relative proteasomal activities (%) among the different expression constructs or strains were compared.

Generation of cell extracts and cell fractionation

$5x10^7$ cells were pelleted by centrifugation. Cell pellets were resuspended in 100 µL of ddH_2O, and cell suspensions were mixed with 100 µL of 0.2 M NaOH (Kushnirov, 2000). After incubation on ice for 15 min, cells were pelleted by centrifugation and resuspended in 100 µL Laemmli sample buffer (2% (w/v) SDS, 10% (v/v) glycerol, 2% (v/v) β-mercapto ethanol, 60 mM Tris-HCl pH 6.8, bromophenol blue). After thorough mixing, cell suspensions were heated for 7 min at 97°C, cooled down on ice, and frozen at -80°C until use.

Isolation of crude mitochondria was performed by differential centrifugation according to (Braun et al., 2009) with minor modifications. Protein concentrations were determined applying Bradford assay. Samples were either directly incubated in Laemmli sample buffer, or precipitated according to (Wessel and Flügge, 1984) and then resuspended in Laemmli sample buffer prior SDS-PAGE.

SDS-PAGE and immunoblot analyses

Tricine-SDS-PAGE and immunoblot analyses were used for protein analyses (Schägger, 2006; Towbin et al., 1979). Cell extracts were thawed at RT and centrifuged for 1 min at 16.000 *g*. 12 µL of supernatant (equivalent to $6x10^6$ cells) were used for separation on 12% Tricine-SDS polyacrylamide gels using a SDS-PAGE separation apparatus (Mini Protean Tetra System, Bio-Rad, Munich, Germany). Protein transfer on PVDF membranes (pore size 0.2 µm, Immuno-Blot PVDF Membrane For Protein Blotting, Bio-Rad) was performed in a wet blotting chamber (Mini Protean Tetra System, Bio-Rad). Membranes were incubated in blocking buffer (5% (w/v) ECL Advance blocking agent [GE Healthcare] for anti-UBB^{+1} or non-fat milk [Carl Roth, Karlsruhe, Germany] for all other antibodies in TBS-T (1% (v/v) Tween-20) for 1 h at RT or overnight at 4°C. The first antibody was diluted in blocking buffer (for the mouse monoclonal antibodies anti-FLAG M2 [1:1,000] [Sigma-Aldrich], anti-ubiquitin [1:8,000] [BD Biosciences, Heidelberg, Germany], and for the rabbit polyclonal antibodies anti-Cdc48 (serum 70) [1:1000 to 1:2500] (Fröhlich et al., 1991), anti-cytochrome *c* [1:1,000] [N. Pfanner], anti-hexokinase [1:15,000], anti-Por1 [1:1,000] [W. Neupert, Munich, Germany], anti-Rip1 [1:2,000] [N. Pfanner], and anti-SSC1 [1:2,000] [N. Pfanner]) and anti-UBB^{+1} [Ubi3, bleeding 050897; 1:1,000] (de Vrij et al., 2001)). Incubation was performed for 1 h at RT or overnight at 4°C. Membranes were washed with TBS-T three times for 10 min, and were then incubated for 1 h at RT with the respective secondary antibody coupled with horseradish peroxidase (goat anti-rabbit IgG or goat anti-mouse IgG

[Promega and Sigma-Aldrich, respectively], diluted 1:10,000 in blocking buffer). Membranes were washed with TBS-T three times for 10 min. Immunodetection was done using either self-made luminol or self-made luminol supplemented with Lumigen TMA-6 (Lumigen, Beckman Coulter, MI, USA). Membranes were incubated for 2 min with luminol solution and were exposed to and digitized in an ImageQuant LAS 4000 (GE Healthcare, Munich, Germany) with the following settings (method: chemiluminescence, exposure time: increment, sensitivity/resolution: standard, high, or super depending on signal strength). Images were processed with Adobe Photoshop CS6 (Adobe).

Immunoblot quantification was done with the gel analysis method in ImageJ 1.47m. Briefly, the peak area (or peak chain area) of the immunosignal of interest (*e.g.* fl-UBB^{+1} detected with anti-UBB^{+1}) was quantified and normalized to the immunosignal of a loading control (*e.g.* hexokinase detected with α-Hxk). Saturated immunosignals or peaks (or peak chains) which could not be discriminated from background signals were discarded. Experiments were repeated at least three times.

Sample preparation for mass spectrometry

Crude mitochondrial extracts were taken up in SDS lysis buffer, thawed, reduced with 1 mM DTT (Sigma-Aldrich) for 5 min at 95°C and alkylated using 5.5 mM iodoacetamide (Sigma-Aldrich) for 30 min at 25°C. Protein mixtures were separated by SDS-PAGE using 4-12% Bis-Tris mini gradient gels (NuPAGE, Invitrogen). The gel lanes were cut into 10 equal slices, which were in-gel digested with trypsin (Promega) (Shevchenko et al., 2006), and the resulting peptide mixtures were processed on STAGE tips as described (Rappsilber et al., 2007).

Mass spectrometry measurements and data analysis

Generation of mass spectrometric raw data and their analyses was performed as described in (Sprenger et al., 2013). Samples analyzed by MS were measured on a LTQ Orbitrap XL mass spectrometer (Thermo Fisher Scientific, Bremen, Germany) coupled to an Eksigent NanoLC-ultra. HPLC-column tips (fused silica) with 75 µm inner diameter were self-packed (Gruhler et al., 2005) with Reprosil-Pur 120 ODS-3 to a length of 20 cm. No pre-column was used. Peptides were injected at a flow of 500 nL/min in 92% buffer A (0.5% acetic acid in HPLC gradient grade water) and 2% buffer B (0.5% acetic acid in 80% acetonitrile, 20% water). Separation was achieved by a linear gradient from 10% to 30% of buffer B at a flow rate of 250 nL/min. The mass spectrometer was operated in the data-dependent mode and switched automatically between MS (max. of 1 $x10^6$ ions) and MS/MS. Each MS scan was followed by a maximum of five MS/MS scans in the linear ion trap using normalized collision energy of 35% and a target value of 5,000. Parent ions with a charge state of z = 1 and unassigned charge states were excluded from fragmentation. The mass range for MS was m/z = 370 to 2,000. The resolution was set to 60,000. MS parameters were as follows: spray voltage 2.3 kV; no sheath and auxiliary gas flow; ion transfer tube temperature 200°C.

The MS raw data files were uploaded into the MaxQuant software version 1.4.0.8. (Cox and Mann, 2008) which performs peak and SILAC-pair detection, generates peak lists of mass error corrected peptides and data base searches (Andromeda search engine). A full length yeast database (UniProt, May 2013, 6,651 entries) containing common contaminants was employed, carbamidomethyl cysteine was set as fixed modification and methionine oxidation and protein amino-terminal acetylation were set as variable modifications. Triple SILAC was chosen as quantitation mode. Three miss cleavages were allowed, enzyme specificity was trypsin/P, and the MS/MS tolerance was set to 0.5 Da. The average mass precision of identified peptides was in general less than 1 ppm after recalibration. Peptide lists

were further used by MaxQuant to identify and relatively quantify proteins using the following parameters: peptide, and protein false discovery rates (FDR) were set to 0.01, maximum peptide posterior error probability (PEP) was set to 0.1, minimum peptide length was set to 6, minimum number peptides for identification and quantitation of proteins was set to two of which one must be unique, minimum peptide ratio count was set to 2, and identified proteins have been re-quantified. The "match-between-run" option (1 min) was used. Perseus version 1.2.0.16. (Cox and Mann, 2008) was used to identify significantly changed proteins ($p < 0.05$) under different treatments.

Extraction of metabolites for targeted metabolomics

Culture aliquots of OD_{600} ~ 20 (from four different yeast clones of each genotype) were harvested by filtration using 0.22 µm sterile filters, washed once (on filter) with 5 mL ddH_2O and immediately quenched by deep-freezing the filters in liquid nitrogen. Filtration and washing step was performed in less than 30 sec until freezing step. Metabolites were extracted by two different methods with extracts obtained from uniformly ^{13}C-labeled (U13C) yeast cells (see below) serving as an internal standard (Istd). U13C-Istd was applied directly on frozen filters prior to extraction. For acid extraction of metabolites, cells (washed directly from frozen filters) were resuspended in 1 mL ice-cold 5% trichloroacetic acid (TCA) and incubated for 1 h on ice with occasionally vortexing. Supernatants (10 min; 10,000 *g*) were lyophilized and resuspended in 200 µL ddH_2O. For extraction with hot ethanol, cells were incubated in 2.5 mL boiling ethanol solution (75% ethanol, 10 mM ammonium acetate) and incubated for 2 min at 96°C. Supernatants were collected, N_2 evaporated to ~ ¼ of initial volume at RT and finally lyophilized and reconstituted in 200 µL ddH_2O. Extracts were stored at -80°C until metabolite measurements were performed with LC/MS.

Total number of cells of each sample was determined after extraction from cell pellets resuspended and appropriately diluted in water using CASY cell counter technology (Roche) in order to normalize the results from the LC/MS measurement.

To generate U13C-Istd, the prototrophic yeast (*S. cerevisiae* strain CEN.PK113-7D) was grown for 24 h or 72 h (an equal mix of the two cultures were used) on uniformly-labeled ^{13}C-glucose as sole carbon source using medium as described above but lacking any amino acids or bases. Acid or ethanol extracts of labeled yeast cells were performed as for unlabeled cells (see above) using 30% methanol as a final solvent and stored at -80°C upon use. 15 µL of this extract served as U13C-Istd for each sample.

Targeted metabolomics

Metabolites were determined using ion pair reversed-phase liquid chromatography coupled to negative electro spray high resolution mass spectrometry (IP-RP-LC/HRMS). The method was adapted with parts from (Bennett et al., 2008; Buescher et al., 2010). All analyses were carried out on an Ultimate 3000 System coupled to an Exactive XL Mass spectrometer (Orbitrap-system, Thermo Fisher Scientific) using an electrospray ion source. The system was controlled by Xcalibur Software 2.2. The HPLC column was an Atlantis T3 3 µm, 150 x 2.1 mm (Waters). Eluent A consisted of 5% MeOH (v/v) in water containing 10 mM tributylamine and 15 mM acetic acid. Eluent B was isopropanol. Table A shows a detailed gradient description.

Metabolites were detected in negative ESI mode using high resolution (R = 50,000). Peak area ratios to uniformly ^{13}C-labeled internal standards (U13C-Istd, see section on *Extraction of Metabolites*) were calculated for relative quantification of the metabolites listed in Table B using Tracefinder Software (Thermo Fisher Scientific).

Table A: HPLC gradient for targeted metabolomics.

Eluent A: 5% MeOH (v/v) in water, 10 mM tributylamine, 15 mM acetic. Eluent B: isopropanol

time [min]	%A	flow rate [µml/min]
0	0	350
7	0	350
11	2	350
12	9	300
16	9	300
18	25	250
19	50	200
32	70	200
34	0	200
36	0	300
37	0	350
39	0	350

Table B: Compounds for relative quantification

Retention time	Compound	unlabeled	^{13}C-labeled
		m/z	m/z
0.67	Ornithine	131.0826	136.0994
0.79	Lysine	145.0983	151.1184
0.85	Arginine	173.1044	179.1245

Immunohistochemistry

Postmortem tissues of hippocampi from AD patients and non-demented controls were obtained from the Netherlands Brain Bank (Amsterdam, The Netherlands) (Table S6) as 6 µm thick paraffin sections. Immunohistochemistry was performed as previously described (Zouambia et al., 2008). Sections were deparaffinated by subsequent treatment with xylene (2x 15 min), ethanol (2x 10 min 100%, 2x 10 min 96%, 10 min 80%, 10 min 70%, and 10 min 60%), and formic acid (30 min). After rinsing in ddH_2O (30 min), and in TBS (3x 10 min), sections were incubated overnight at 4°C with antibodies against misfolded tau (MC1, Peter Davies, NY, USA, mouse monoclonal, 1:100), UBB^{+1} (Ubi2A, rabbit polyclonal,

1:500) (Fischer et al., 2003), VMS1 (ANKZF1, ab94790, Abcam, rabbit polyclonal, 1:500), and VDAC1 (ab14734, Abcam, mouse monoclonal, 1:500). All dilutions were in SUMI buffer [50 mM Tris buffered saline with 0.25 % (w/v) gelatine and 0.5 % (v/v) Triton X-100, pH 7.6]. After rinsing in TBS (3x 10 min), sections were incubated for 1 h at RT with biotinylated secondary donkey anti-mouse or donkey anti-rabbit antibodies (Jackson Laboratories, Bar Habor, Main, U.S.A; 1:400 in SUMI buffer), followed by washing in TBS-T/TBS/TBS-T (10 min each), and by incubation for 1 h at RT with avidin-biotin-peroxidase complex (ABC, Vector Labs, Brunschwig Chemie, Amsterdam, The Netherlands, 1:400 in TBS-T). After washing in TBS (2x 10 min), and incubation with Tris buffer (50 mM Tris-HCl, pH 7.6, 10 min), sections were stained with Tris-buffered 3,3'-diaminobenzidine (DAB) intensified by 0.04 % (w/v) nickel chloride (pH 7.6) for 5 to 20 min, dependent on antibody and background staining. Staining was stopped by incubation in ddH_2O (3x 10 min), and sections were mounted on glass slides. After drying overnight, sections were dehydrated by subsequent treatment with ethanol (3 min 50%, 3 min 60%, 3 min 70%, 3 min 80%, 2x 3 min 96%, 2x 10 min 100%), Ultraclear (3x 10 min, Mallinokrodt Baker B.V., Deventer, The Netherlands), and coverslipped with Pertex mounting media (Leica Biosystems).

Statistics

For statistics SigmaPlot V13 (Systat Software, Erkrath, Germany) was used. For comparing two groups, either unpaired two-tailed Student's t-test with ad hoc normality and equal variance tests, or paired two-tailed Student's t-tests with ad hoc normality tests were applied. Rank Sum Tests were used for comparing two groups if ad hoc tests failed. For comparing many groups One Way ANOVA or One Way Repeated Measures ANOVA with ad hoc normality and equal variance tests, and post hoc tests (Dunn's, Holm-Sidak, Bonferroni methods) were applied. If ad hoc tests failed, ANOVA on Ranks or Repeated Measures ANOVA on Ranks were used with post hoc tests (Dunn's, Tuckey methods).

Differences were considered to be marked with p-values < 0.1 and significant with p-values ≤ 0.05. If not other stated, error bars indicate the standard errors of the mean or percent change values obtained from the independent experiments. For details see Figure legends and Table S1.

Supplemental References

Bennett, B.D., Yuan, J., Kimball, E.H., and Rabinowitz, J.D. (2008). Absolute quantitation of intracellular metabolite concentrations by an isotope ratio-based approach. Nat Protoc *3*, 1299-1311.

Braun, R.J., Kinkl, N., Zischka, H., and Ueffing, M. (2009). 16-BAC/SDS-PAGE analysis of membrane proteins of yeast mitochondria purified by free flow electrophoresis. Methods Mol Biol *528*, 83-107.

Braun, R.J., Sommer, C., Carmona-Gutierrez, D., Khoury, C.M., Ring, J., Büttner, S., and Madeo, F. (2011). Neurotoxic 43-kDa TAR DNA-binding Protein (TDP-43) Triggers Mitochondrion-dependent Programmed Cell Death in Yeast. J Biol Chem *286*, 19958-19972.

Buescher, J.M., Moco, S., Sauer, U., and Zamboni, N. (2010). Ultrahigh performance liquid chromatography-tandem mass spectrometry method for fast and robust quantification of anionic and aromatic metabolites. Anal Chem *82*, 4403-4412.

Büttner, S., Bitto, A., Ring, J., Augsten, M., Zabrocki, P., Eisenberg, T., Jungwirth, H., Hutter, S., Carmona-Gutierrez, D., Kroemer, G., *et al.* (2008). Functional mitochondria are required for alpha-synuclein toxicity in aging yeast. J Biol Chem *283*, 7554-7560.

Büttner, S., Eisenberg, T., Carmona-Gutierrez, D., Ruli, D., Knauer, H., Ruckenstuhl, C., Sigrist, C., Wissing, S., Kollroser, M., Fröhlich, K.U., *et al.* (2007). Endonuclease G regulates budding yeast life and death. Mol Cell *25*, 233-246.

Büttner, S., Ruli, D., Vogtle, F.N., Galluzzi, L., Moitzi, B., Eisenberg, T., Kepp, O., Habernig, L., Carmona-Gutierrez, D., Rockenfeller, P., *et al.* (2011). A yeast BH3-only protein mediates the mitochondrial pathway of apoptosis. EMBO J *30*, 2779-2792.

Chondrogianni, N., Georgila, K., Kourtis, N., Tavernarakis, N., and Gonos, E.S. (2014). 20S proteasome activation promotes life span extension and resistance to proteotoxicity in *Caenorhabditis elegans*. FASEB J *71*, 303-320.

Cox, J., and Mann, M. (2008). MaxQuant enables high peptide identification rates, individualized p.p.b.-range mass accuracies and proteome-wide protein quantification. Nat Biotechnol *26*, 1367-1372.

de Pril, R., Fischer, D.F., Maat-Schieman, M.L., Hobo, B., de Vos, R.A., Brunt, E.R., Hol, E.M., Roos, R.A., and van Leeuwen, F.W. (2004). Accumulation of aberrant ubiquitin induces aggregate formation and cell death in polyglutamine diseases. Hum Mol Genet *13*, 1803-1813.

de Pril, R., Fischer, D.F., Roos, R.A., and van Leeuwen, F.W. (2007). Ubiquitin-conjugating enzyme E2-25K increases aggregate formation and cell death in polyglutamine diseases. Mol Cell Neurosci *34*, 10-19.

de Pril, R., Hobo, B., van Tijn, P., Roos, R.A., van Leeuwen, F.W., and Fischer, D.F. (2010). Modest proteasomal inhibition by aberrant ubiquitin exacerbates aggregate formation in a Huntington disease mouse model. Mol Cell Neurosci *43*, 281-286.

Fischer, D.F., De Vos, R.A., Van Dijk, R., De Vrij, F.M., Proper, E.A., Sonnemans, M.A., Verhage, M.C., Sluijs, J.A., Hobo, B., Zouambia, M., *et al.* (2003). Disease-specific accumulation of mutant ubiquitin as a marker for proteasomal dysfunction in the brain. FASEB J *17*, 2014-2024.

Fröhlich, K.U., Fries, H.W., Rüdiger, M., Erdmann, R., Botstein, D., and Mecke, D. (1991). Yeast cell cycle protein CDC48p shows full-length homology to the mammalian protein VCP and is a member of a protein family involved in secretion, peroxisome formation, and gene expression. J Cell Biol *114*, 443-453.

Gruhler, A., Olsen, J.V., Mohammed, S., Mortensen, P., Faergeman, N.J., Mann, M., and Jensen, O.N. (2005). Quantitative phosphoproteomics applied to the yeast pheromone signaling pathway. Mol Cell Proteomics *4*, 310-327.

Heessen, S., Dantuma, N.P., Tessarz, P., Jellne, M., and Masucci, M.G. (2003). Inhibition of ubiquitin/proteasome-dependent proteolysis in *Saccharomyces cerevisiae* by a Gly-Ala repeat. FEBS Lett *555*, 397-404.

Irmler, M., Gentier, R.J., Dennissen, F.J., Schulz, H., Bolle, I., Holter, S.M., Kallnik, M., Cheng, J.J., Klingenspor, M., Rozman, J., *et al.* (2012). Long-term proteasomal inhibition in transgenic mice by UBB(+1) expression results in dysfunction of central respiration control reminiscent of brainstem neuropathology in Alzheimer patients. Acta Neuropathol *124*, 187-197.

Jarosch, E., Taxis, C., Volkwein, C., Bordallo, J., Finley, D., Wolf, D.H., and Sommer, T. (2002). Protein dislocation from the ER requires polyubiquitination and the AAA-ATPase Cdc48. Nat Cell Biol *4*, 134-139.

Kushnirov, V.V. (2000). Rapid and reliable protein extraction from yeast. Yeast *16*, 857-860.

Madeo, F., Fröhlich, E., Ligr, M., Grey, M., Sigrist, S.J., Wolf, D.H., and Fröhlich, K.U. (1999). Oxygen stress: a regulator of apoptosis in yeast. J Cell Biol *145*, 757-767.

Ohlmeier, S., Kastaniotis, A.J., Hiltunen, J.K., and Bergmann, U. (2004). The yeast mitochondrial proteome, a study of fermentative and respiratory growth. J Biol Chem *279*, 3956-3979.

Prokisch, H., Scharfe, C., Camp, D.G., 2nd, Xiao, W., David, L., Andreoli, C., Monroe, M.E., Moore, R.J., Gritsenko, M.A., Kozany, C., *et al.* (2004). Integrative analysis of the mitochondrial proteome in yeast. PLoS Biol *2*, e160.

Rappsilber, J., Mann, M., and Ishihama, Y. (2007). Protocol for micro-purification, enrichment, pre-fractionation and storage of peptides for proteomics using StageTips. Nat Protoc *2*, 1896-1906.

Reinders, J., Zahedi, R.P., Pfanner, N., Meisinger, C., and Sickmann, A. (2006). Toward the complete yeast mitochondrial proteome: multidimensional separation techniques for mitochondrial proteomics. J Proteome Res *5*, 1543-1554.

Ruenwai, R., Neiss, A., Laoteng, K., Vongsangnak, W., Dalfard, A.B., Cheevadhanarak, S., Petranovic, D., and Nielsen, J. (2011). Heterologous production of polyunsaturated fatty acids in *Saccharomyces cerevisiae* causes a global transcriptional response resulting in reduced proteasomal activity and increased oxidative stress. Biotechnol J *6*, 343-356.

Schägger, H. (2006). Tricine-SDS-PAGE. Nat Protoc *1*, 16-22.

Sherman, F. (2002). Getting started with yeast. Methods Enzymol *350*, 3-41.

Shevchenko, A., Tomas, H., Havlis, J., Olsen, J.V., and Mann, M. (2006). In-gel digestion for mass spectrometric characterization of proteins and proteomes. Nat Protoc *1*, 2856-2860.

Sickmann, A., Reinders, J., Wagner, Y., Joppich, C., Zahedi, R., Meyer, H.E., Schonfisch, B., Perschil, I., Chacinska, A., Guiard, B.*, et al.* (2003). The proteome of *Saccharomyces cerevisiae* mitochondria. Proc Natl Acad Sci U S A *100*, 13207-13212.

Sprenger, A., Weber, S., Zarai, M., Engelke, R., Nascimento, J.M., Gretzmeier, C., Hilpert, M., Boerries, M., Has, C., Busch, H.*, et al.* (2013). Consistency of the proteome in primary human keratinocytes with respect to gender, age, and skin localization. Mol Cell Proteomics *12*, 2509-2521.

Towbin, H., Staehelin, T., and Gordon, J. (1979). Electrophoretic transfer of proteins from polyacrylamide gels to nitrocellulose sheets: procedure and some applications. Proc Natl Acad Sci U S A *76*, 4350-4354.

van Tijn, P., Hobo, B., Verhage, M.C., Oitzl, M.S., van Leeuwen, F.W., and Fischer, D.F. (2011). Alzheimer-associated mutant ubiquitin impairs spatial reference memory. Physiol Behav *102*, 193-200.

Wessel, D., and Flügge, U.I. (1984). A method for the quantitative recovery of protein in dilute solution in the presence of detergents and lipids. Anal Biochem *138*, 141-143.

Westermann, B. (2010). Mitochondrial fusion and fission in cell life and death. Nat Rev Mol Cell Biol *11*, 872-884.

Zouambia, M., Fischer, D.F., Hobo, B., De Vos, R.A., Hol, E.M., Varndell, I.M., Sheppard, P.W., and Van Leeuwen, F.W. (2008). Proteasome subunit proteins and neuropathology in tauopathies and synucleinopathies: Consequences for proteomic analyses. Proteomics *8*, 1221-1236.

Detailed Author Contributions

Figure/Table	Designed the experiment	Performed the experiment	Analyzed the data	Prepared the figure/ table
Figure 1A-C	R.J.B.	K.P.	R.J.B., K.P.	R.J.B., C.S.
Figure 1D	R.J.B.	R.J.B.	R.J.B.	R.J.B., C.S.
Figure 2A-F	R.J.B.	R.J.B.	R.J.B.	R.J.B., C.S.
Figure 3A+C+E	R.J.B.	R.J.B.	R.J.B.	R.J.B., C.S.
Figure 3B+F	R.J.B.	C.S., R.J.B.	C.S., R.J.B.	R.J.B., C.S.
Figure 3D	R.J.B.	C.L., R.J.B.	C.L., R.J.B.	R.J.B., C.S.
Figure 4A	R.J.B., C.S.	R.J.B., C.S.	R.J.B., C.S.	R.J.B., C.S.
Figure 4B	R.J.B.	R.J.B.	R.J.B.	R.J.B., C.S.
Figure 4C-E	C.S., R.J.B.	C.S.	C.S., R.J.B.	R.J.B., C.S.
Figure 4F+G	R.J.B.	K.P.	R.J.B., K.P., C.L.	R.J.B., C.S.
Figure 4H	R.J.B., C.S.	C.S., R.J.B.	C.S., R.J.B.	R.J.B., C.S.
Figure 4I	R.J.B.	R.J.B.	R.J.B.	R.J.B., C.S.
Figure 5A	F.M., J.D., R.J.B.	V.I.D., K.P.	V.I.D., R.J.B.	R.J.B., C.S.
Figure 5B	R.J.B.	C.L.	C.L., R.J.B.	R.J.B., C.S.
Figure 5C	F.M., T.E., C.M., C.S., R.J.B.	C.S., T.E., G.T.	T.E., C.S., G.T.	R.J.B., C.S.
Figure 5D	-	-	-	R.J.B., C.S.
Figure 5E	F.M., C.S., R.J.B.	C.S.	C.S., R.J.B.	R.J.B., C.S.
Figure 5F+G	F.M., C.S., R.J.B.	L.H.	L.H., R.J.B.	R.J.B., C.S.
Figure 6A-C	R.J.B.	R.J.B., C.L.	R.J.B., C.L.	R.J.B., C.S.
Figure 6D-F	F.M., C.S.	C.S.	C.S., R.J.B.	R.J.B., C.S.
Figure 6G-I	C.S., R.J.B.	C.S.	C.S., R.J.B.	R.J.B., C.S.
Figure 6J	F.M., J.D., R.J.B.	V.I.D., K.P.	V.I.D., R.J.B.	R.J.B., C.S.
Figure 6K	F.M., T.E., C.M., C.S., R.J.B.	C.S., T.E., G.T.	T.E., C.S., G.T.	R.J.B., C.S.
Figure 7A-D	F.W.v.L., R.J.B.	R.J.B., R.J.G.G.	R.J.G.G., F.W.v.L., R.J.B.	F.M., C.S., R.J.B.
Figure S1A+B	R.J.B.	K.P.	R.J.B., K.P.	R.J.B., C.S.
Figure S1C	R.J.B.	R.J.B.	R.J.B.	R.J.B., C.S.
Figure S2A-E	R.J.B.	R.J.B.	R.J.B.	R.J.B., C.S.
Figure S3A	R.J.B.	C.S., R.J.B.	C.S., R.J.B.	R.J.B., C.S.
Figure S3B	R.J.B.	C.L., R.J.B.	C.L., R.J.B.	R.J.B., C.S.
Figure S3C	R.J.B.	C.L., R.J.B.	C.L., R.J.B.	R.J.B., C.S.
Figure S3D-K	R.J.B.	C.L.	C.L.	R.J.B., C.S.
Figure S4A	R.J.B.	R.J.B.	R.J.B.	R.J.B., C.S.
Figure S4B+C	R.J.B.	K.P.	R.J.B., K.P.	R.J.B., C.S.
Figure S4D	R.J.B., C.S.	C.S., R.J.B.	C.S., R.J.B.	R.J.B., C.S.
Figure S4E	R.J.B.	R.J.B.	R.J.B.	R.J.B., C.S.
Figure S4F-H	R.J.B.	K.P.	R.J.B., K.P.	R.J.B., C.S.
Figure S4I	R.J.B.	R.J.B.	R.J.B.	R.J.B., C.S.
Figure S5A	R.J.B.	C.L.	C.L., R.J.B.	R.J.B., C.S.
Figure S5B	F.M., C.S., R.J.B.	C.S.	C.S., R.J.B.	R.J.B., C.S.
Figure S6A-C	R.J.B.	R.J.B., C.L.	R.J.B., C.L.	R.J.B., C.S.
Figure S6D	F.M., C.S.	C.S.	C.S., R.J.B.	R.J.B., C.S.
Figure S6E-H	R.J.B.	C.L.	C.L.	R.J.B., C.S.
Figure S6I+J	R.J.B.	K.P.	C.L.	R.J.B., C.S.
Figure S7	F.W.v.L., R.J.B.	R.J.B., R.J.G.G.	R.J.G.G., F.W.v.L., R.J.B.	R.J.B., F.M., C.S.
Table S1	-	-	-	R.J.B.
Tables S2-S4	F.M., J.D., R.J.B.	V.I.D., K.P.	V.I.D., R.J.B.	R.J.B.
Tables S5+S6	F.W.v.L., R.J.B.	R.J.B., R.J.G.G.	R.J.G.G., F.W.v.L., R.J.B.	R.J.B., F.W.v.L.